Aalto University

OPEN ACCESS

This is an electronic reprint of the original article.
This reprint may differ from the original in pagination and typographic detail.

Mousa, Hossam H. H.; Mahmoud, Karar; Lehtonen, Matti

Enhancing Renewable Energy Hosting Capacity in Unbalanced Microgrids via Empowering Smart Inverters

Published in:
IEEE Access

DOI:
10.1109/ACCESS.2025.3533043

Published: 01/01/2025

Document Version
Publisher's PDF, also known as Version of record

Published under the following license:
CC BY

Please cite the original version:
Mousa, H. H. H., Mahmoud, K., & Lehtonen, M. (2025). Enhancing Renewable Energy Hosting Capacity in Unbalanced Microgrids via Empowering Smart Inverters. *IEEE Access*, *13*, 17161-17181. https://doi.org/10.1109/ACCESS.2025.3533043

This material is protected by copyright and other intellectual property rights, and duplication or sale of all or part of any of the repository collections is not permitted, except that material may be duplicated by you for your research use or educational purposes in electronic or print form. You must obtain permission for any other use. Electronic or print copies may not be offered, whether for sale or otherwise to anyone who is not an authorised user.

IEEE Access
Multidisciplinary ⋮ Rapid Review ⋮ Open Access Journal

Received 8 January 2025, accepted 21 January 2025, date of publication 23 January 2025, date of current version 29 January 2025.

Digital Object Identifier 10.1109/ACCESS.2025.3533043

RESEARCH ARTICLE

Enhancing Renewable Energy Hosting Capacity in Unbalanced Microgrids via Empowering Smart Inverters

HOSSAM H. H. MOUSA[1,2], KARAR MAHMOUD[3], (Senior Member, IEEE), AND MATTI LEHTONEN[1,4]

[1]Department of Electrical Engineering and Automation, Aalto University, 00076 Espoo, Finland
[2]Department of Electrical Engineering, South Valley University, Qena 83523, Egypt
[3]Department of Electrical Engineering, Aswan University, Aswan 81542, Egypt
[4]Department of Engineering Sciences in the Electrical Field, Constanta Maritime University, 900663 Constanta, Romania

Corresponding author: Hossam H. H. Mousa (Hossam.mousa@aalto.fi)

This work was supported in part by the Department of Electrical Engineering and Automation, Aalto University, Espoo, Finland; and in part by the Ministry of Research, Innovation, and Digitalization under Project PNRR-C9-I8-760111/23.05.2023 and Project CF 48/14.11.2022. The work of Hossam H. H. Mousa was supported by the Full Scholarship (Long-Term Mission System) from the Ministry of Higher Education and Scientific Research of the Arab Republic of Egypt.

ABSTRACT This article presents a coordinated planning strategy for renewable energy sources (RESs) and energy storage systems (ESSs) in unbalanced microgrids. The approach aims to mitigate voltage unbalance, reduce power losses, alleviate feeder congestion, and maximize the hosting capacity (HC) of RESs in grid-connected unbalanced microgrids. By employing smart inverter control for photovoltaic (PV) and ESS inverters, the strategy enhances the integration of additional RESs while minimizing power exchange between operational zones and the utility grid (UG). To achieve such an ambitious goal, smart inverter control functions are employed, including combined mode, volt-var (VV), volt-watt (VW) for Photovoltaic (PV) inverters, and VW for ESS inverters. The IEEE 123-bus test system, divided into six operational zones, is used as a case study, incorporating plug-in electric vehicle (PEV) demand and wind-based distributed generation (DG). A metaheuristic algorithm is developed for optimal DG and ESS deployment using MATLAB and OpenDSS. The results demonstrate significant improvements, including a 16% reduction in feeder congestion, a 150% increase in PV penetration, a 13% reduction in power losses, and decreased reliance on the UG, ensuring enhanced power quality and system reliability.

INDEX TERMS Distributed generation, energy storage systems, hosting capacity, renewable energy sources, voltage unbalance.

NOMENCLATURE

LIST OF ABBREVIATIONS

CAES	Compressed Air Energy Storage.
DG	Distributed Generation.
DR	Demand Response.
DSM	Demand Side Management strategies.
ESSs	Energy Storage Systems.
FACTS	Flexible AC Transmission Systems.
HC	Hosting Capacity.
MESs	Multi-Carrier Energy Systems.
MOGWO	Multi-objective Grey Wolf Optimization algorithm.
MPPT	Maximum Power Point Tracking.
MPSs	Modern Power Systems.
PDF	Probability Density Function.
PEV	Plug-in Electric Vehicle.
PV	Photovoltaic.
RESs	Renewable Energy Sources.
UG	Utility Grid.
UPF	Unity Power Factor.
VUI	Voltage Unbalance Index.
VV	Volt-Var.
VW	Volt-Watt.

The associate editor coordinating the review of this manuscript and approving it for publication was Guillaume Parent.

© 2025 The Authors. This work is licensed under a Creative Commons Attribution 4.0 License.
For more information, see https://creativecommons.org/licenses/by/4.0/

WECS	Wind Energy Conversion System.
WT	Wind Turbine.

LIST OF SYMBOLS

i_d and i_q	The d-axis and q-axis currents of the PV inverter (A).
i_r	Rated current of the PV inverter (A).
V_a, V_b and V_c	The phase voltages of the PV inverter (kV).
V_{ga}, V_{gb} and V_{gc}	Grid phase voltages (kV).
i_a, i_b and i_c	Grid phase currents (A).
(V_{gd}, V_{gq}) and (V_d, V_q)	The d-axis and q-axis of the grid voltages and PV inverter voltages, respectively (kV).
R_f and L_f	The filter resistance and inductance, respectively.
$V_{cut\ in}$	Cut-in wind speed (m/s).
$V_{cut\ out}$	Cut-out wind speed (m/s).
P_m	Captured mechanical power from WECS (kW).
β_{ref}	Pitch angle (degree).
VUI	Voltage unbalance index (%).
I_{OL}	Overloading of main feeders(%).
λ_{pv}	Penetration level of PV systems (%).
f_t	Complete objective function.
θ	Vector of the decision variables.
$Max.AVD$	Maximum average voltage deviation.
$V_i^{avg.}$	Average voltage of the three phases in (V) and $i$presents the bus number.
N_f	Total number of selected main feeders.
S_t^{pv} , and S_t^{load}	Total apparent power of integrated PVs, and connected loads, respectively (kVA).
P_{Load}^i and Q_{Load}^i	Active and reactive powers of load (kW, kvar) connected in bus i, respectively.
N_L	Total number of loads.
P_{Loss}^l and Q_{Loss}^l	Active and reactive power losses per line, respectively (kW, kvar).
P_{ESS}^k	Active power of ESSs at each zone (kW).
P_{Grid} and Q_{Grid}	Swapped active and reactive power from the UG, respectively (kW, kvar).
SoC_t	State of charge of ESSs (%).
P_{Ess}^{ch}, P_{Ess}^{dis}	Charging/discharging power of ESSs (kW).
U_{ch}^t, U_{dis}^t	Flag bits of charging and discharging modes.
i_d and i_q	The d-axis and q-axis currents of the PV inverter (A).
i_r	Rated current of the PV inverter (A).
V_a, V_b and V_c	The phase voltages of the PV inverter (kV).
V_{ga}, V_{gb} and V_{gc}	Grid phase voltages (kV).

I. INTRODUCTION

Recently, the necessity for clean and sustainable energy sources, such as renewable energy sources (RESs), has become crucial to mitigate the adverse impacts of conventional energy sources, including climate change and carbon emissions [1]. Consequently, RESs are being extensively integrated into modern power systems (MPSs), especially microgrids, to meet electrical demands, as illustrated in Fig. 1. It is evident that hydropower contributes the largest share, followed by wind and photovoltaic (PV) energy. Despite their significant benefits, numerous challenges remain in coordinating their continuous integration [2].

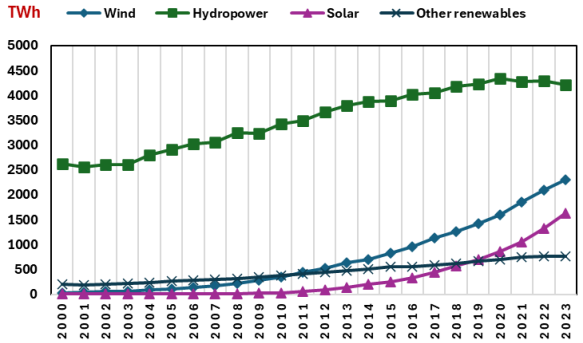

FIGURE 1. Global energy generation by RESs [3].

A. BACKGROUND AND MOTIVATION

Distributed generation (DG) units are proposed as small-scale power generation units implemented near consumption areas to enhance power quality without requiring significant modifications to the utility grid (UG) infrastructure. DGs are classified into renewable energy sources (RESs) and non-RESs [4]. Although DGs are employed to enhance power system reliability and flexibility, they can also introduce adverse impacts, particularly those based on RESs. These impacts include power quality issues such as voltage fluctuations, voltage unbalance, and power loss due to the dispatchable and intermittent nature of RESs, complicating forecasting and placement [5]. Additionally, the use of power electronic devices in these technologies can reduce power system inertia after DG connections and influence power system transients, leading to increased harmonics and frequency instability [6], [7]. Similarly, the integration of single-phase DGs can cause significant power loss and overloading of transformers and lines, leading to voltage imbalance. These

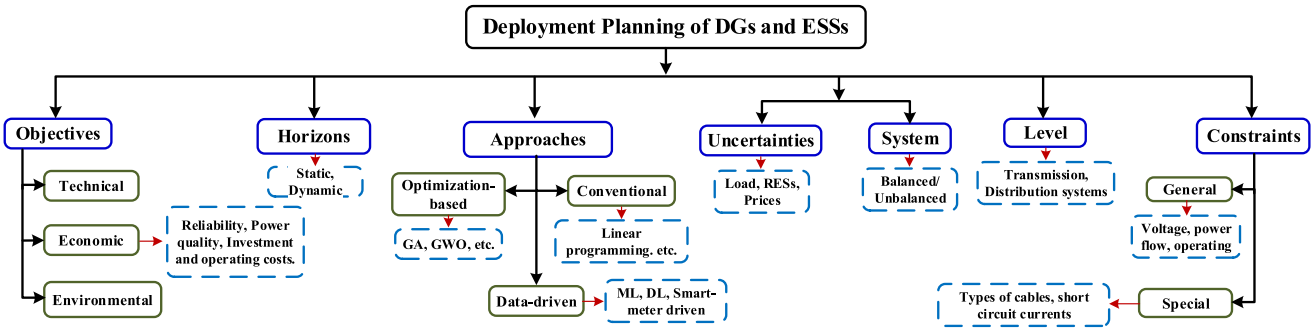

FIGURE 2. Comprehensive planning aspects for deploying DGs and ESSs.

issues also affect protection systems such as relays, reducing overall power system reliability. Therefore, it is necessary to optimally allocate DGs within MPSs with complete controllability to maintain energy balance between generation and demand, which is a challenging task [8].

To cope with the adverse impacts of DGs, energy storage systems (ESSs) are effective solutions to energy storage and exchange in request to maintain acceptable operational levels of power quality in MPSs [2]. ESSs can be classified into several types such as electrical, chemical, and mechanical, among others [9]. ESSs alleviate feeder congestion, improve power quality, reduce power loss, smooth power fluctuations, increase DG penetration, enhance system reliability, provide virtual inertia, and maximize financial efficiency [10]. Despite these benefits, several factors must be considered, such as investment cost, type, lifetime, environmental impact, and others, especially in large-scale implementations, which pose challenges for power system planners. Therefore, it is essential to coordinate the deployment of both DGs and ESSs in the planning process. This not only enhances power quality but also increases power system reliability and flexibility under different operational conditions.

To deal with these challenges, the hosting capacity (HC) concept is used to describe the increased integration of DGs, ESSs, electric vehicles (EVs), and other technologies into MPSs without violating any operational performance indices [11], [12]. Various approaches are applied to calculate HC, such as deterministic, stochastic, optimization-based, and data-driven methods, each with its own features and drawbacks. The calculated HC of MPSs provides the maximum limit for the penetration of various industrial technologies, which can be achieved by implementing enhancement techniques such as voltage violation mitigation strategies, demand-side management strategies, DGs and ESSs deployment, network reconfiguration, and energy sector coupling. The concept of HC is crucial for planners and system operators to effectively manage the increased integration of new technologies and facilitate power exchange.

B. LITERATURE REVIEW

To address power quality issues in MPSs and microgrids due to the increased penetration of new industrial technologies, it is crucial to implement accurate planning strategies [13]. These strategies must consider economic, technical, and environmental aspects. This need arises because most UGs have not fully upgraded their infrastructure to accommodate these new technologies. Therefore, proper planning ensures that the integration of technologies like DGs and ESSs can be managed effectively, minimizing disruptions and maintaining system reliability [2].

Fig.2 illustrates the most important planning aspects for deploying the DGs and ESSs. These aspects involve:

- **Applied approaches**: deterministic, stochastic, optimization-based, and data-driven approaches.
- **Objectives**: enhancing power quality, reliability, and flexibility while minimizing costs and environmental impacts.
- **Planning levels**: transmission, distribution, and microgrid levels.
- **Constraints**: technical constraints like voltage limits, power losses, and system stability, as well as economic and environmental constraints.

According to the literatures [2], [13], [14], [15], [16], and [17], the integration of DGs, ESSs, and other technologies through the planning process has introduced various power quality issues. These issues can be categorized into voltage-related problems such as voltage unbalance, sag, swell, flicker, and distortion in voltage profiles; frequency variations and harmonics; power losses and high thermal ampacity overloading; protection issues; power factor and energy curtailment; and other technical and economic factors. To address these problems, the optimal planning and deployment of these technologies should be considered, along with advanced monitoring, metering, and communication systems. In this regard, various strategies are applied to enhance power quality and increase the HC of the MPSs. These strategies include voltage mitigating techniques such as passive, active, and hybrid filters, and Flexible AC Transmission Systems (FACTS) [12].

Additionally, network configuration adjustments, Demand Side Management (DSM) strategies, and Demand Response (DR) programs are effective methods for solving these issues, supported by advanced control schemes.

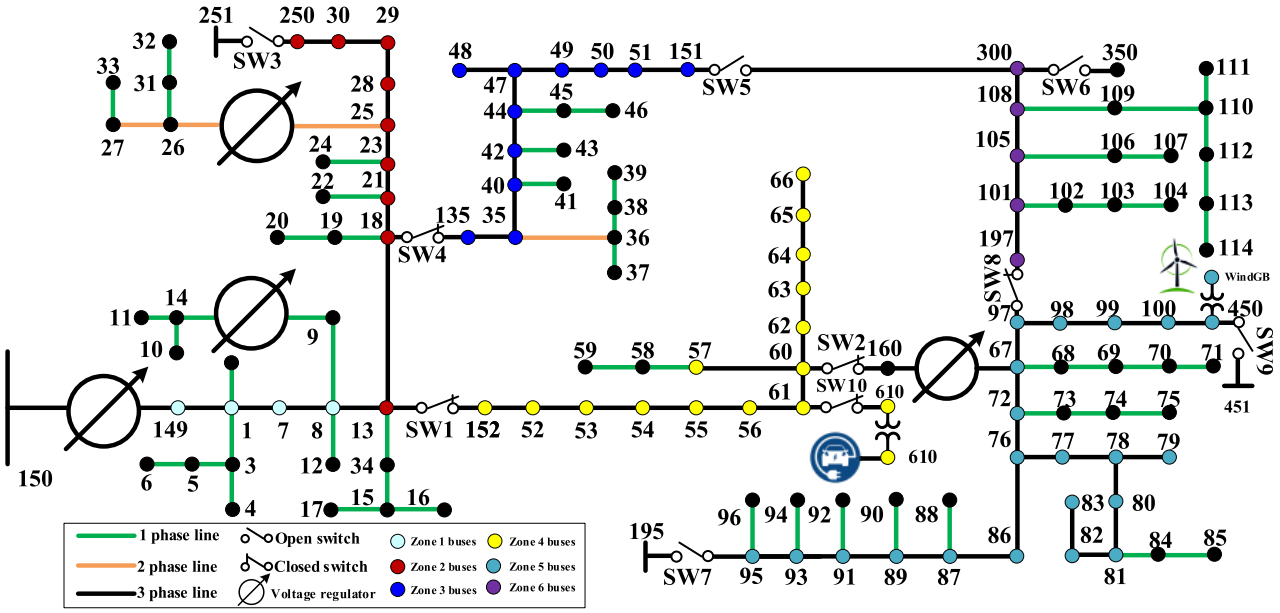

FIGURE 3. Proposed planning structure of IEEE 123 bus distribution system.

To deal with various power quality issues such as voltage deviation, power loss, etc. in cost-effective and environmental methods, various articles proposed optimal allocation strategies of DGs using many objectives and different types of planning approaches and algorithms [17], [18], [19], [20], [21], [22], [23], [24], [25], [26], [27]. However, many challenges appeared due to the bidirectional power flow such as reserve power flow, high fault currents, flicker, and harmonic. Additionally, the intermittent nature of allocated DGs with load variations influences power system reliability and flexibility. Therefore, ESSs are implemented to address these problems, especially reducing thermal line loading. In [28], [29], [30], [31], [32], [33], [34], [35], [36], [37], and [38], coordinated planning of DGs (RESs and others), and ESSs were proposed to deal with various challenges as mentioned previously. Additionally, providing energy management methods to cope with generation and load uncertainties in cost-effective approaches. Some of these articles proposed planning strategies for DGs and ESSs to enhance the HC of the studied systems without other power quality improvement objectives [18], [22], [31], [38]. The literature shows the importance of coordinating planning for deploying DGs and ESSs to address various power quality issues which lead to increasing the HC of MPSs. The complete literature is discussed in Table 1 including main objectives, system configuration, findings, and specifications of planning strategies.

C. MAIN CONTRIBUTIONS

Regarding the previous literature review, there are several challenges in the coordinated allocation of DGs and ESSs in distribution systems. Most reviewed articles assume that the studied systems have a radial configuration, and are balanced, whereas practical systems are often unbalanced. Some planning strategies do not consider objectives such as voltage unbalance, which becomes apparent in large-scale systems like the IEEE 123-bus and 8500-bus systems.

Furthermore, most articles do not address cable/line congestion, which refers to the overloading or excessive use of electrical cables. This can lead to potential performance issues, overheating, increased resistance, voltage drops, and reduced efficiency, ultimately necessitating careful planning and management to ensure reliable and safe operation. Additionally, the reactive power capacity and smart functionalities of inverters are often overlooked. It is important to note that, to achieve the best planning results, it is essential to consider all of the previous aspects. As shown in the literature, the simultaneous consideration of such practical terms is not investigated deeply, which is the scope of this work.

To fill the gap in the literature, in this article, previous challenges are addressed here in terms of enhancing the power quality and increasing the HC. Thus, the main contribution can be illustrated as;

- It proposes a coordinated deployment planning of PVs (bus, kW) and ESSs (bus, kW, kWh) at each zone, taking into account power quality issues.
- The planning strategy addresses several objectives, including the reduction of voltage and current unbalance, power losses, and congestion and overloading of the main feeders. Additionally, it aims to maximize the HC of the microgrid to accommodate more DGs in each partitioned area, and to reduce dependency on the UG alongside enhancing system reliability and efficiency.

TABLE 1. Literature analysis of most recent published articles related to deployment planning of DGs, and ESSs.

Ref.	Year	Studied system	Objectives	Planning tool			Type of DG/ESS	Main contributions
				Applied approach	Algorithm	software		
[18]	2018	IEEE 123-bus test system	HC of PV	Conv.	Linear programming	Python, GAMS	PV	Increasing the PV HC in distribution systems considering power quality issues.
[17]		IEEE 33 bus distribution system	power loss, voltage profile, power congestion	Optz.	Grey wolf optimization (GWO)	-	P/Q type DGs	Optimal allocation of DGs using various optimization algorithms.
[20]	2019	IEEE 32-bus test system and two real distribution test systems	Line losses, costs	Conv.	MC	OpenCL	WT, PV	Enhancing the handling process of multi-objective DG allocation planning problem compared to other metaheuristic approaches.
[28]	2020	IEEE 69-bus distribution system	loss minimization, voltage, and loadability improvement	Optz.	Particle swarm optimization (PSO)	-	PV, ESS	Optimal sizing of PV and ESSs with annual static/dynamic network reconfigurations
[29]	2021	IEEE 33 and 69-bus distribution systems	Power and energy losses		Rider optimization algorithm (ROA)	MATLAB	WT, PV, biomass, ESSs	Optimal sizing of DGs and ESSs with considering generation uncertainties.
[31]		IEEE 30-bus test system	HC of RES, network partitioning and optimal operational planning issues	Conv./Optz.	-	GAMS, DIgSILENT PowerFactory	WT, PV, ESSs	
[32], [33]		Microgrids	Operating costs		depends			
[21]		33-node radial distribution network	Voltage profile, power loss, overall cost	Optz.	Grey Wolf algorithm and Harris Hawks algorithm (GWA-HHA)	MATLAB	PV, ESS, EV charging stations	Allocation of PVs, EV charging stations, and ESSs with uncertainties to enhance the power quality.
[22]		Medium voltage distribution system	HC of RESs, system reliability, total annual operating cost		Geographical information system multi-criteria decision-making method (GIS-MCDM)	Python with ArcPy	PV	Optimal allocation of PVs to enhance the power quality and decrease the annual operating cost.
[23]		IEEE 33- and 69-bus radial distribution systems	Emission, power quality, power loss, energy cost		Enhanced grey wolf optimizer and particle swarm optimization (EGWO-PSO)	MATLAB	Gas turbine, PV, WT	Placement of capacitor banks and DGs to achieve minimum energy cost and emission with acceptable levels of power quality.
[34]	2022	Microgrids	Energy management, investment costs		Genetic algorithm (GA)	-	PV, ESSs	Optimal sizing of PV and ESSs besides energy management strategy during load shedding.
[35]		IEEE 33-bus distribution system	Energy management, ESS investment costs, power losses, flicker emission and voltage deviation		Crow search algorithm (CSA)	MATLAB	WT, PV, ESSs	Optimal allocation of PV,WT, and ESSs besides energy management strategy.
[36]			Power losses and voltage fluctuations	Conv./Optz	NSGA-II optimization and the multi-objective particle swarm optimization (MOPSO) algorithm	-		
[37]	2023		Energy management, operating costs, and emission	Optz.	Hybrid particle swarm and grey wolf optimizer	MATLAB	DG, ESS, multi-energy carrier systems	Placement of DSTATCOM, ESSS and DGs to achieve minimum energy cost and emission with acceptable levels of power quality.
[38]			HC of RESs, voltage fluctuations, cost,and power disturbances		GA	MATLAB, GAMS	RESs, ESSs	Optimal allocation of ESSs to increase the HC of distribution systems.
[24]		IEEE 33- and 62-bus radial distribution systems	Voltage profile, power loss	Optz.	Dingo Optimization Algorithm	MATLAB	PV	Optimal placement of PVs to solve power quality issues under diverse loading operations.
[25]		IEEE 33- and 85-bus radial distribution systems	Power loss		Artificial ecosystem-based optimization–opposition-based learning (AEO-OBL)		PV, WT	Optimal allocation of DGs to reduce the power losses.
[26]		IEEE 33-bus distribution system and Portugal (94-bus network)	Emission, voltage deviation, power quality, power loss, energy cost		Artificial hummingbird algorithm (AHA)		Gas turbine, PV, WT	Placement of DGs to achieve minimum energy cost and emission with acceptable levels of power quality.
[27]		IEEE 123-bus distribution system	Voltage profile, power loss		Equilibrium Optimizer (EO) algorithm	MATLAB/Simulink, IEEE-PES data, and OpenDSS	DGs	Enhancing the solving methodology for DG allocation problem.
[19]	2024	Various distribution systems	Power losses, cost, computational time		Mathematical Programming Language (AMPL)	GAMS	DGs	Minimizing costs and losses by DG allocations with load variations.
[30]		IEEE 33-bus distribution system	Voltage violations and excessive network losses	Optz./data-driven	Combined	-	PV, ESSs	Network configuration method for PV and ESSs to solve power quality issues.

*Conventional: Conv.; Monte Carlo: MC; Wind turbine: WT; Optimization-based: Optz.;

- Varying HC utilization across operational zones of microgrids without violation of the HC limits according to international standards.
- Optimal smart inverter control and functions are applied to inverters coupled with PVs (operating in combined mode, volt-var (VV), and volt-watt (VW)) and ESSs (operating in VW). PV inverters are equipped with reactive power capability to support the partitioned area until they reach their full capacity, after which they are controlled to provide only active power.
- The study considers the uncertainties of demand and generation along with the dispatchable curve of ESSs.
- This study examines an unbalanced three-phase system, specifically the IEEE 123-bus grid-connected

TABLE 2. General IEEE 123-bus microgrid structure.

General configuration				
No. of buses	**No. of lines**	**No. of loads**		
123	124	1 ph	2 ph	3 ph
		85	3	3
Wind-based DG	Bus#450, kV=0.69 at #WindGB, rated power = 1500 kW at unity power factor (UPF)			
PEVs	Bus#610, kV=0.48, rated power = 2000 kW			

TABLE 3. Operational zones of modified IEEE 123-bus microgrid.

Zone	Candidate buses at each zone	Main feeder	Bus connections		Amp. rating
			Bus 1	Bus 2	
Z#1	[149, 1, 7, 8]	Line#115	#149	#1	400 A
Z#2	[13, 18, 21, 23, 25, 28, 29, 30, 250]	Line#13	#13	#18	400 A
Z#3	[35, 40, 42, 44, 47, 48, 49, 50, 51, 135, 151]	Line#114	#135	#35	400 A
Z#4	[52, 53, 54, 55, 56, 57, 60, 61, 62, 63, 64, 65, 66, 152]	Line#116	#152	#52	400 A
Z#5	[67, 72, 76, 77, 78, 79, 80, 81, 82, 83, 86, 87, 89, 91, 93, 95, 97, 98, 99, 100, 450]	Line#117	#160r	#67	400 A
Z#6	[101, 105, 108, 197, 300]	Line#118	#197	#101	400 A

unbalanced microgrid, which is divided into six operational zones. Each zone contains candidate unbalanced three-phase buses for the strategic placement of PV systems and ESSs. The majority of plug-in EV (PEV) demand is concentrated in the residential sector, connected to Bus #610, with a wind-based DG connected to Bus #450.

- The multi-objective grey wolf optimization (MOGWO) algorithm is applied to solve the planning problem due to its demonstrated superiority over other algorithms as mentioned in [17].

D. ARTICLE ORGANIZATION

Following the introduction, section II introduces the proposed methodology for coordinated deployment planning of PVs and ESSs in unbalanced distribution systems, detailing system configuration, performance indices, constraints, and standards. The applied planning strategy is outlined in section III, with simulation results presented in section IV. This is followed by concluding with the work's summary in section V.

II. MATHEMATICAL PROBLEM FORMATION

A. MODIFIED IEEE 123-BUS CONFIGURATION

This study is conducted on an unbalanced three-phase system, specifically the IEEE 123-bus microgrid, as illustrated in Fig. 3 and detailed in Table 2, and Table 3 [39]. To represent the grid-connected microgrids, the system is divided into six operational zones, with each zone containing candidate unbalanced three-phase buses for selecting the strategic placement of PV systems and ESSs. The bulk of PEV demand is considered in the residential sector which is assumed connected to Bus#610 through a 3 MVA load transformer. Furthermore, wind-based DG with 1.5 MW is connected to Bus#450 through a 2 MVA transformer. The total active and reactive powers of loads are 3490 kW and 1920 kvar, respectively, classified into single, two, and three-phase loads. The load consumption varies stochastically per day, as illustrated in Fig. 4. Besides, most common components found in actual distribution systems, such as voltage regulators, shunt capacitor banks, and switches. Several DGs and ESSs are allocated to this system, and their modelling will be discussed subsequently.

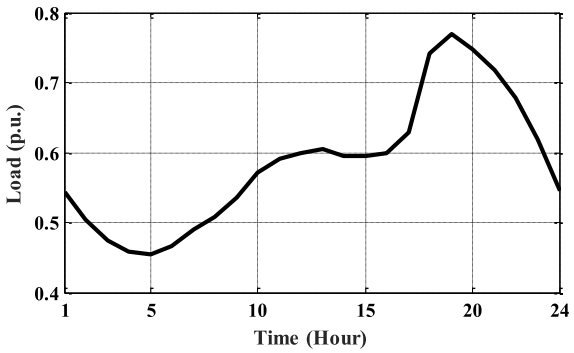

FIGURE 4. Load consumption profile per day.

B. DESCRIPTION OF SYSTEM COMPONENTS

In this subsection, the detailed modeling and operation of utilized DGs, PEVs and ESSs are discussed below.

1) PV-BASED DG MODELLING

The PV systems produce power while the PV inverters are responsible for regulating its generations according to the grid requirements. The PV array consists of a group of PV panels each consisting of a PV cell that converts the solar energy into DC power. The common modelling of PV cells is described using one diode model which is highly accurate with fewer components implementation, as depicted in Fig.5. The complete mathematical modelling is given in [40] and [41].

The PV generation system is connected to the grid via a PV inverter, which manages the injection of active and reactive power, and maintains the DC bus voltage according to reference values based on weather variations. The DC voltage is regulated using a DC voltage control loop. Additionally, the active and reactive power injected into the grid is controlled through a current control loop that adjusts the d-axis and q-axis currents to ensure optimal performance, as illustrated in Eq. (1) [40], [41].

$$i_d = \begin{cases} i_r & \forall pf = 1 \\ < i_r & \forall pf < 1 \end{cases} \quad \Big| \quad i_q = \begin{cases} 0 & \forall pf = 1 \\ \sqrt{i_r^2 - i_d^2} & \forall pf < 1 \end{cases} \tag{1}$$

where, i_r is the rated current of the PV inverter. The phase voltages (V_a, V_b and V_c) of the PV inverter are determined in Eq. (2).as a function of grid voltages (V_{ga}, V_{gb} and V_{gc}) and currents (i_a, i_b and i_c),

$$\begin{bmatrix} V_a \\ V_b \\ V_c \end{bmatrix} = [R_f] \begin{bmatrix} i_a \\ i_b \\ i_c \end{bmatrix} + \begin{bmatrix} \dot{\lambda_a} \\ \dot{\lambda_b} \\ \dot{\lambda_c} \end{bmatrix} + \begin{bmatrix} V_{ga} \\ V_{gb} \\ V_{gc} \end{bmatrix} \tag{2}$$

where $\dot{\lambda_a} = L_f \frac{di_{fa}}{dt}$, $\dot{\lambda_b} = L_f \frac{di_{fb}}{dt}$ and $\dot{\lambda_c} = L_f \frac{di_{fc}}{dt}$, R_f and L_f are the filter resistance and inductance, respectively. By transforming Eq. (3) from the *abc* frame to the *dq* frame, the grid voltages are expressed as:

$$\begin{bmatrix} V_{gd} \\ V_{gq} \end{bmatrix} = \begin{bmatrix} V_d \\ V_q \end{bmatrix} - [r_f] \begin{bmatrix} i_d \\ i_q \end{bmatrix} - \begin{bmatrix} \dot{\lambda_d} - \omega_g \psi_q \\ \dot{\lambda_q} + \omega_g \psi_d \end{bmatrix} \tag{3}$$

where (V_{gd}, V_{gq}) and (V_d, V_q) are the d-axis and q-axis of the grid voltages and PV inverter voltages, respectively. $\omega_g = 2\pi f_g$, $\psi_q = l_f i_q$, $\psi_d = l_f i_d$, $\dot{\lambda_d} = l_f \frac{d}{dt} i_d$, $\dot{\lambda_q} = l_f \frac{d}{dt} i_q$. The instantaneous active and reactive power injected by the PV inverter to the grid are given by:

$$P_g = \frac{3}{2}(V_{gd} i_d - V_{gq} i_q) \tag{4}$$

$$Q_g = \frac{3}{2}(V_{gd} i_q - V_{gq} i_d) \tag{5}$$

Recently, modern PV inverters have been designed with reactive power capability to adjust the voltage level. Therefore, their sizing should be larger than the nominal rate of the installed PV system (i) enabling them to provide reactive power at time (t) within the limit of their apparent power S_i^{rate}, as given in Eq. (6).

$$Q_{i,t}^{\lim} = \pm \sqrt{\left(S_i^{rate}\right)^2 - \left(P_{i,t}\right)^2} \tag{6}$$

For controlling the integrated PV inverters, the reactive power capability requirements for PV systems are specified in IEEE 1547-2018 [42]. To satisfy the IEEE 1547-2018 standard, the smart inverter will have the capability to inject/absorb a minimum of 44% reactive power [43]. Hence, the smart inverters have several features to regulate the active and reactive power exchange in different modes with different constraints, as depicted in Fig.6 (a). In this study, the PV inverters are controlled using combined modes including volt-var (VV), and volt-watt (VW) modes. In which, the power exchanged with the grid will be the required active power, which might be limited by the VW function, and the reactive power requested by the VV function. By using VV control mode for the applied PV inverters with the same parameters, the reactive power (generated/absorbed) is regulated according to the operating voltage, depicted in Fig.6 (b) which is formulated as,

$$Q(V_{act.}) = \begin{cases} Q_{max} & \forall V_{act.} \le V_1 \\ \left(\frac{V - V_{act.}}{V - V_1}\right) * Q_{\max} & \forall V_1 \le V_{act.} \le V \\ \left(\frac{V - V_{act.}}{V - V_2}\right) * Q_{\min} & \forall V \le V_{act.} \le V_2 \\ Q_{\min} & \forall V_2 \le V_{act.} \end{cases} \tag{7}$$

Furthermore, the active power according to the operating voltage can be adjusted using the VW function, as shown in Fig.6 (c) which is formulated as,

$$P(V_{act.}) = \begin{cases} P_{max} & \forall V_{act.} \le V_1 \\ \left(\frac{V_2 - V_{act.}}{V_2 - V_1}\right) * P_{\max} & \forall V_1 \le V_{act.} \le V_2 \\ 0 & \forall V_2 \le V_{act.} \end{cases} \tag{8}$$

In the daily simulation based on the real data, the solar irradiance and temperature curves for PVs are applied, as depicted in Fig. 7 (a) and (b), respectively. While the stochastic behaviour of wind speed and solar irradiance (X), it is crucial to analyze the probabilities which can be demonstrated using a Weibull probability density function (PDF) [44], [45], [46],

$$f_W(X) = \frac{K}{C}\left(\frac{X}{C}\right)^{K-1} e^{\left(-\left(\frac{X}{C}\right)^K\right)} \tag{9}$$

where C is the scale parameter and K is the shape parameter. Fig.7 (c) shows the solar irradiance distribution obtained from these measurements and includes the Weibull PDF corresponding to the measured data.

Additionally, the effects of temperature and inverter efficiency are considered, as shown in Fig. 8 (a) and (b), respectively. The study assumes that the smallest PV array that can be added is 10 kVA, with increments of the same magnitude until the optimal sizing is determined for the candidate bus. The PV inverters are centrally regulated using the same controller operating in VV-VW modes, with the parameters provided in Table 4.

2) AGGREGATED ESS MODELLING

In In this article, it is assumed that each operational zone is equipped with an aggregated ESS, which may include various types such as batteries, flywheels, compressed air energy storage (CAES), hydrogen, and others. The electrical modelling of these different ESS types is discussed in detail

in [47]. The dispatchable curve for all integrated ESSs is shown in Fig.9 (a). In both charging and discharging modes, ESSs follow a per-unit dispatchable curve. When the curve value is positive, all units discharge at the specified rate. When the curve value is zero, all units remain idle. When the curve value is negative, all units charge at the specified rate according to the curve. Moreover, the ESSs are regulated using smart inverters with the VW function in both charging and discharging modes, as depicted in Fig.9 (b, c), respectively. The technical characteristics of both the ESSs and their inverters are provided in Table 5.

3) WIND-BASED DG MODELLING

In this article, the wind-based DG is assumed to be connected to Bus#450 through a transformer (#WindGB) with a nominal rated power of 1500 kW at UPF, as detailed in Table 6 [48]. Wind generation is based mainly on wind speed variations which are intermittent and unpredictable. Thus, the operating regions illustrate the relationship between wind speed and the output mechanical power. The total captured mechanical power can be categorized into four regions, which are limited between the cut-in wind speed ($V_{cut\ in}$) and the cut-out wind speed ($V_{cut\ out}$):

- **Region 1 and Region 4:** The wind turbine (WT) is stationary for safety reasons.
- **Region 2:** Known as the Maximum Power Point Tracking (MPPT) region, where the WT achieves optimal power output below the rated wind speed.
- **Region 3:** The pitch control region, where mechanical power is regulated to reduce mechanical stress on the WT blades when wind speeds exceed the rated wind speed.

Generally, the captured mechanical power from the wind energy conversion system (WECS) operating regions is formulated as,

$$P_m = \begin{cases} 0 \quad \forall V_{wind} \le V_{cut\ in}, V_{cut\ out} \le V_{wind} \\ P_{rated}\left(\dfrac{V_{wind} - V_{cut\ in}}{V_{rated} - V_{cut\ in}}\right) \quad \forall V_{cut\ in} \le V_{wind} \le V_{rated} \\ P_{rated} \quad \forall V_{rated} \le V_{wind} \le V_{cut\ out} \end{cases} \tag{10}$$

In the MPPT region, the WT is regulated to capture the maximum possible power below the rated wind speed. To achieve this, the pitch angle is set to zero, ensuring the WT blades face the wind directly. Hence, the maximum power can be harvested by adjusting the rotor speed to track the variation in wind speed. In opposition, in the pitch control region, the output power must be mechanically controlled to protect against high wind speeds, particularly sudden gusts. This involves adjusting the pitch angle of the WT blades when the wind speed exceeds the rated level. The pitch control concept is described as follows,

$$\beta_{ref} = \begin{cases} \beta_0 = 0, 0 < \omega_m < \omega_{rated} \\ \dfrac{\Delta\beta}{\Delta\omega_m}(\omega_m - \omega_{rated}) + \beta_0, \omega_m > \omega_{rated} \end{cases} \tag{11}$$

Below the rated wind speed, the pitch angle is set to zero to maximize power output. Above the rated wind speed, the pitch controller limits the rotor speed and can also act as a braking system if rotor speed control is not achieved.

To reflect the realistic variations of wind speed, a 24-hour real wind speed profile is obtained from the wind tower at the National Renewable Energy Laboratory (NREL) National Wind Technology Center (NWTC) [49]. The tower is located at a latitude of 39.91° N, a longitude of 105.23° W, and an elevation of 1855 meters. The wind power is obtained with an average wind speed of 5.1 m/s, recorded at one-hour intervals over one day, as shown in Fig.10 (a).

Real wind speed data was collected through measurements taken at the analyzed location over the period of one day. Fig.10 (b) shows the wind speed distribution obtained from these measurements and includes the Weibull PDF corresponding to the measured data. The wind speed samples generated according to the Weibull PDF are used to model the uncertainty in the WT output power. These generated wind speed samples are then converted into WT output power based on the WT characteristics. Hence, the daily generated power from the WT is illustrated in Fig.10 (c). It is assumed that the MPPT algorithm tracks optimally 100% of maximum power.

4) PEV MODELLING

This study assumes that a significant number of PEVs are connected to the microgrid at Bus #610 through a 3 MVA

TABLE 4. PV array and inverter properties.

kVA limits	10 kVA to 2500 kVA
kV	4.16
%cutin= %cutout	0.1
$\lvert kvar\ (max.)\rvert$	750 $kvar$
Vmin(pu)	0.9
Vmax(pu)	1.03
Nominal irradiance and temperature	1200 W/m^2 & 25°C

TABLE 5. ESS and inverter properties.

Nominal voltage	4.16 kV
Max. power rated	2000 kW
kWh rated (max)	6000
%cutin= %cutout	0.1
PF	1
Vmin(pu)	0.9
Vmax(pu)	1.03
%reserve	20
%stored	100
%idlingkW	2
Rate of charge /discharge %	50% of kW
Inverter efficiency	Fig.8 (b)
Dispatchable curve	Fig.9 (a)
Charge Trigger	Dispatchable curve
Discharge Trigger	

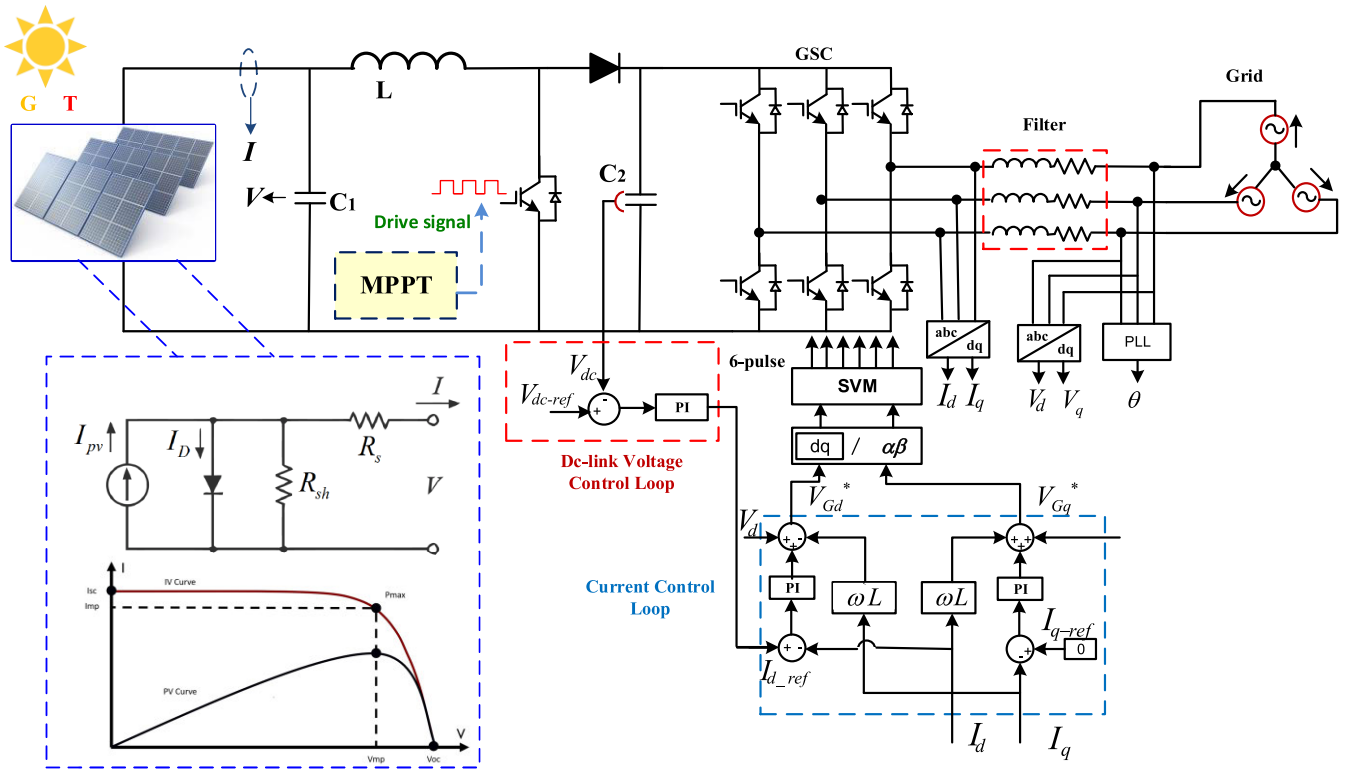

FIGURE 5. Configuration of grid-connected PV system.

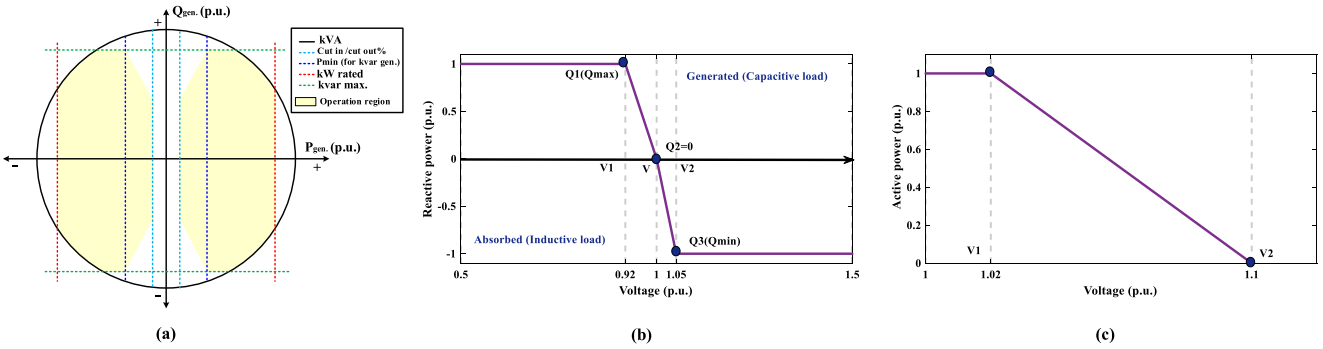

FIGURE 6. General Inverter Capability Curve and is smart functions.

load transformer to analyze their impact on the power grid and to plan the necessary infrastructure. The PEV load profile is used to reflect the realistic operation of PEVs, considering various uncertainties such as vehicle mobility, charging infrastructure, the market share of PEVs, and different parameter sets, as estimated in [47]. In this study, a substantial PEV load (2000 kW) with Level (1) residential charging is integrated into the microgrid based on the per-unit estimated load profile, as depicted in Fig. 11.

C. OBJECTIVE FUNCTION

The objective functions formulated in this study play a critical role in enhancing the HC of RESs in unbalanced microgrids. By minimizing the voltage unbalance index (VUI%) and overloading of main feeders (I_{OL}%), the model ensures stable and reliable grid operation, essential for integrating higher levels of RESs without compromising power quality. Controlling VUI% helps maintain voltage stability within acceptable limits, reducing the risk of adverse effects on equipment and grid performance, as outlined in the EN 50160 standard. Similarly, limiting the feeder loading to within standard capacity mitigates risks such as overheating and efficiency loss, which are common challenges with increased DG penetration. Furthermore, the model maximizes the penetration level (λ_{pv}%) of PV systems, aligning with distribution system operator (DSO) guidelines for optimal DG integration. By balancing these three objectives, the model facilitates an effective and accurate approach to optimize the HC of RESs, supporting

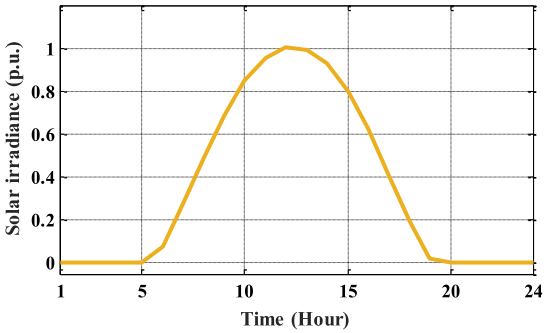

a. Solar irradiance (p.u.) of 1200 W/m2

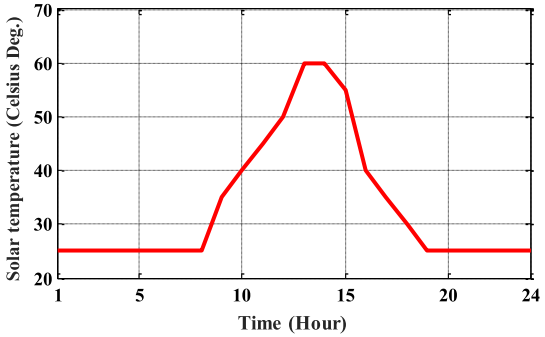

b. Solar temperature in °C

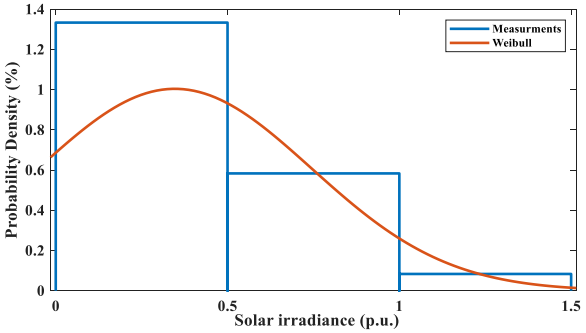

c. Histogram of solar irradiance data and Weibull distribution.

FIGURE 7. Operational weather profiles of PV-based DGs.

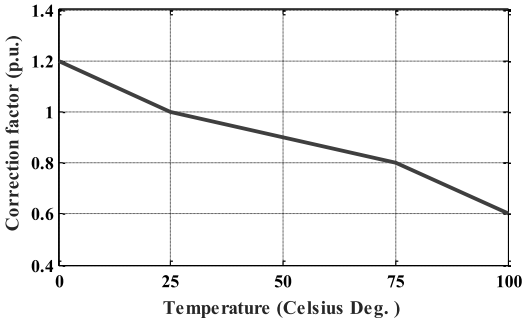

a. Correction factor vs Temperature

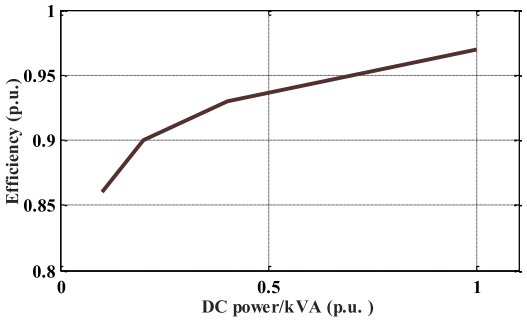

b. Inverter efficiency curve

FIGURE 8. PV array properties.

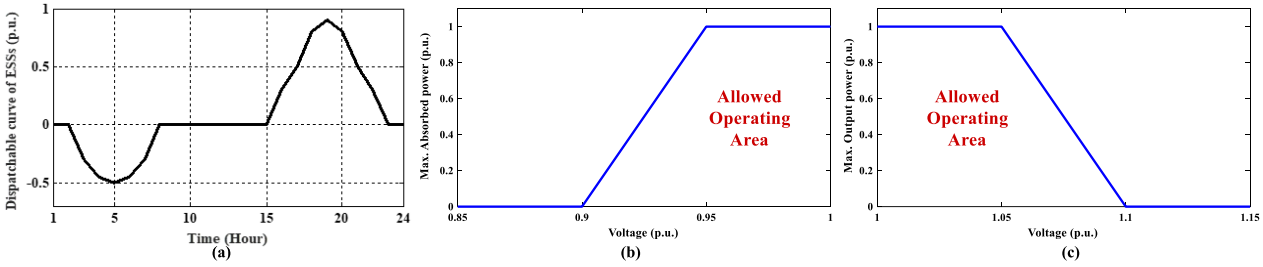

FIGURE 9. Dispatchable curve and VW functions for ESSs.

the development of resilient, efficient, and high-penetration RESs in distribution networks. The complete objective function (f_t) is expressed as shown in Eq. (12).

$$\min_{\theta} \{f_t = w_1 f_1 + w_2 f_2 - w_3 f_3\}$$
$$\text{s.t. } w_1 + w_2 + w_3 = 1 \tag{12}$$

where θ is the vector of the decision variables. $\{f_1, f_2, f_3\}$ are the three objective functions, which are the VUI%, I_{OL}%, and λ_{pv}%, respectively. Additionally, $\{w_1, w_2, w_3\}$ are the

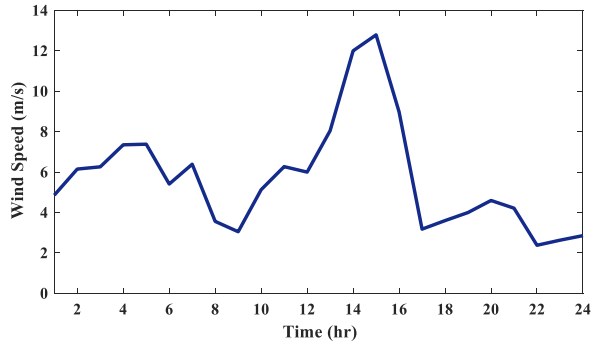

a. Wind speed.

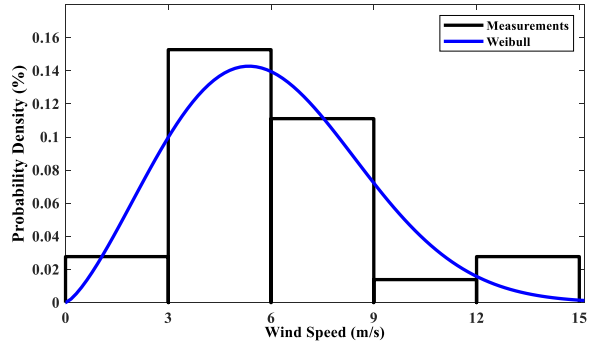

b. Histogram of wind data and Weibull distribution.

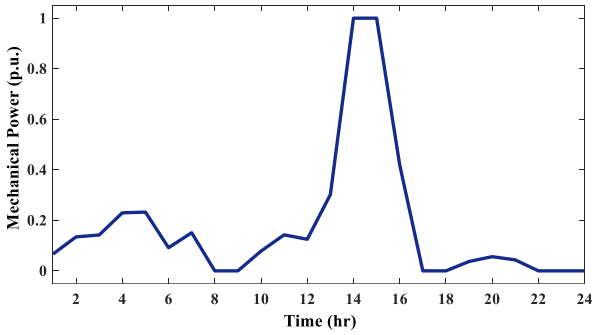

c. Generated output power.

FIGURE 10. Wind-based DG characteristics.

set of weighting factors are defined by the decision maker regarding the planning requirements. For simplicity, the three objectives are weighed equally during optimal planning. The formulations of these 3 subfunctions are bellowed.

1) VUI FORMULATION

The voltage unbalance can be determined using symmetrical voltage components methods or the National Electrical Manufacturers Association (NEMA) definition which is applied in this article [50]. To determine the VUI ratio, the following equation can be applied,

$$f_1 = VUI\% = \frac{Max.AVD}{V_i^{avg.}} * 100\% \tag{13}$$

where $Max.AVD$ is the maximum average voltage deviation from the average voltage of the three phases ($V_i^{avg.}$), $i$presents

TABLE 6. Specification of WT.

The coefficients C1 to C6	$C_1 = 0.5176$ $C_2 = 116$ $C_3 = 0.4$ $C_4 = 5$ $C_5 = 21$ $C_6 = 0.0068$
Blade radius	$R = 35.25\ m$
Air density	$\rho = 1.225 kg/m^3$
Optimal tip speed ratio	$\lambda_{opti} = 8.1$
Maximum power Coefficient	$C_{p-max} = 0.48$
Rated power	$P = 1.5\ MW$
PF	UPF
Transformer WindGB	phases=3, windings=2, buses=(#450 #WindGB), conns.=(delta, wye), kV=(4.16, 0.69), kVA=(2000, 2000), taps='1. 1', XHL=0.5

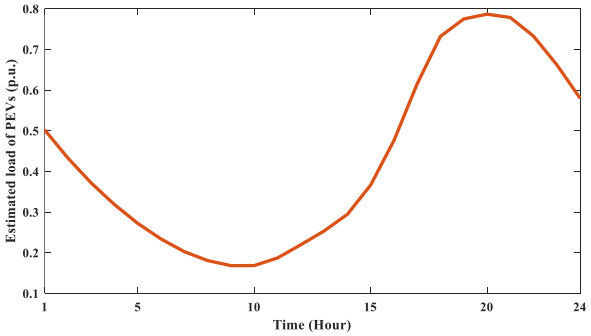

FIGURE 11. Estimated load profile of PEVs per weekday.

the bus number. Both $Max.AVD$, and $V_i^{avg.}$ are expressed as follows,

$$Max.AVD = max. \begin{cases} 3 \\ ph = 1 \end{cases} \left| V_i^{avg.} - V_i^{ph} \right| \tag{14}$$

$$V_i^{avg} = \frac{1}{3}(V_i^a + V_i^b + V_i^c) \tag{15}$$

where V_i^{ph} is the actual voltage per phase (V_i^a, V_i^b, V_i^c). Although voltage imbalance in the distribution system is usually minor, the VUI% should be kept within 2%, as EN 50160 standard recommended.

2) AMPACITY OF FEEDERS

With the increased penetration of DGs, feeders may become overloaded, exceeding their nominal ampacity. This can lead to various adverse effects, such as increased voltage drop, overheating, reduced efficiency, and potential failures and deterioration. Therefore, it is crucial for planners to consider the ampacity of service feeders to ensure reliable and safe operation when integrating new DGs. The feeder ampacity shouldn't exceed 100% or 150% of nominal feeder ratting regarding EN 50160 and VDE-AR-N 4105 standards, respectively. I_{OL}% of the main feeder at each zone is calculated as,

$$I_{OL}\% = \frac{Max. \begin{cases} 3 \\ ph = 1 \end{cases} |I_{act}.per\ phase|}{|I_{rate}|} * 100\% \tag{16}$$

Thus,

$$f_2 = \sum_{i=1}^{N_f} max(\mathrm{I_{OL}}\%\forall zone) \tag{17}$$

where, N_f is the total selected main feeders overall the operational zones.

3) PENETRATION LEVEL

To ensure that the power quality indices not be violated, the penetration level of PV-based DGs is considered in the objective function to be maximized. The penetration level ($\lambda_{pv}\%$) is expressed as,

$$f_3 = \lambda_{pv}\% = \frac{S_t^{pv}}{\mathrm{S_t^{load}}} * 100\% \tag{18}$$

where, S_t^{pv} , $\mathrm{S_t^{load}}$ are the total apparent power of integrated PVs, and the total apparent power of connected loads, respectively, at 100% loading condition. According to the DSO rules of thumb, it is recommended that the integrated DG size should be between 50% and 100% of the feeder capacity [11], [12]. The proposed planning model can be a helpful tool to determine the best PV size within the accepted range with high accuracy rates.

D. OPERATIONAL CONSTRAINTS

1) POWER FLOW BALANCE CONSTRAINTS

The power flow balance constraints presented in Eqs. (19) and (20) ensure that the system's power supply matches the demand and losses, taking into account all active and reactive power sources, including loads, renewable generation (PV and wind), ESSs, and EVs. Specifically, these constraints prevent issues like voltage deviations, feeder overloads, and energy storage over-discharge, which are critical for maintaining stable system operation. The selected constraints align with common industry practices and regulatory standards, such as IEEE 1547-2018, which emphasizes reliable operation of distributed energy resources without compromising grid stability. Eqs. (19, 20) are formualted as,

$$\sum_{i=1}^{N_L} P_{Load}^{i}(t) + \sum_{l=1}^{N_{line}} P_{Loss}^{l}(t) - P_{wind}(t) - \sum_{k=1}^{N_Z} P_{pv}^{k}(t) \pm \sum_{k=1}^{N_Z} P_{ESS}^{k}(t) + P_{EV}(t) = P_{Grid}(t) \tag{19}$$

$$\sum_{i=1}^{N_L} Q_{Load}^{i}(t) + \sum_{l=1}^{N_{line}} Q_{Loss}^{l}(t) \pm \sum_{k=1}^{N_z} Q_{pv}^{k}(t) = Q_{Grid}(t) \tag{20}$$

where P_{Load}^{i} and Q_{Load}^{i} are the active and reactive powers of load connected in bus i to the total number of loads (N_L), P_{Loss}^{l} and Q_{Loss}^{l} state the active and reactive power losses per line, $P_{ESS}^{k}$is the active power of ESSs at each zone, and P_{Grid} and $Q_{Grid}$are the swapped active and reactive power from the UG.

2) VOLTAGE LIMITS

According to EN 50160 and ANSI C84.1 standards, the voltage limits should be in the range of $\pm 10\%$ of V_{rated} for load busses, and $\pm 5\%$ of V_{rated} for PV-based DG feeders, respectively, as given in Eqs. (21,22).

$$0.9 \leq V_i^{load} \leq 1.1(p.u.) \tag{21}$$

$$0.95 \leq V_i^{DG} \leq 1.05(p.u.) \tag{22}$$

3) CONSTRAINTS OF PV-BASED DGS

The installed PV systems not only inject active power but also have reactive power capability. This is achieved by controlling the PV inverters using a combined mode operation (VV-VW) to adjust the required reactive power. The selected apparent power size is constrained as follows:

$$10\ kVA \leq S_{pv}^{k} \leq 2500\ kVA \tag{23}$$

Hence, the PV inverters are regulated to absorb/inject the reactive in demand with limits,

$$-750\ kvar \leq Q_{pv}^{k} \leq 750\ kvar \tag{24}$$

4) FEEDER CURRENT LIMITS

The maximum ampacity of the main feeders in each zone should be within the limits specified by the following equation:

$$I_{act.} \leq I_{max.} \tag{25}$$

5) ESS CONSTRAINTS [51], [52]

The state of charge (SoC) of ESSs is restricted as,

$$SoC_{min} \leq SoC_t \leq SoC_{max} \tag{26}$$

where the charging/discharging power of ESSs is kept within limits,

$$P_{Ess}^{ch} \leq P_{Ess}^{t} \leq P_{Ess}^{dis} \tag{27}$$

To ensure the correct operation mode of ESSs at any given time, flag bits are used, as both charging and discharging modes cannot occur simultaneously,

$$U_{ch}^{t} + U_{dis}^{t} \leq 1;\ s.t. U_{ch}^{t}, U_{dis}^{t} \in \{0, 1\} \tag{28}$$

Other constraints are mentioned in Table 5.

III. PROPOSED PLANNING METHODOLOGY

In this section, the proposed planning methodology is explained in terms of the applied software, and the planning strategy using MOGWO algorithm.

A. CO-SIMULATION BETWEEN OPENDSS AND MATLAB

In [12], a comparison is made among various software platforms used for solving Optimal Power Flow (OPF) problems. The study highlights the characteristics, advantages, and drawbacks of each platform, providing a comprehensive evaluation of their performance in power system optimization tasks. This comparison is valuable for understanding the

strengths and limitations of different software tools, helping researchers and practitioners select the most suitable platform for their specific needs in OPF analysis. Various studies have utilized OpenDSS, MATLAB, or co-simulation between these platforms to solve complex and large-scale distribution system problems [27], [53]. These studies typically focus on analyzing power flow, optimization, and other system performance metrics in unbalanced and modern distribution networks. Their results reveal key differences in performance, such as computational speed, accuracy, and flexibility in handling dynamic and unbalanced conditions. Comparisons across these studies highlight the strengths of OpenDSS in modeling distribution systems and running simulations, while MATLAB is often preferred for its powerful optimization algorithms and ability to handle large data sets. Co-simulation approaches, combining both platforms, leverage the strengths of each, but also introduce challenges in coordination and data exchange between systems.

Hence, the proposed methodology is validated using two platforms, OpenDSS and Matlab. The OpenDSS software is a powerful, flexible, and reliable research platform that can implement the OPF problem efficiently and rapidly. However, the OpenDSS doesn't have the ability to change the variables data and rebuild the admittance (Y) matrix at every iteration. Therefore, Matlab is combined to coordinate the control of OpenDSS and manage the optimization problem by providing the new variable's data to OpenDSS to make OPF problem and then analyze the upcoming at from the OpenDSS. Which offers accurate data processing speed, as depicted in Fig.12.

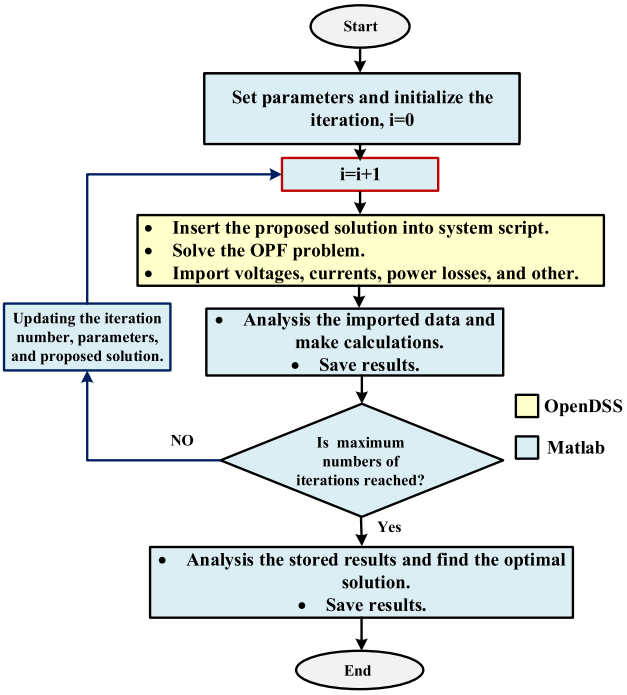

FIGURE 12. Detailed co-simulation between Matlab and OpenDSS.

B. OPTIMAL PLANNING STRATEGY USING MOGWO ALGORITHM

The MOGWO algorithm is used to optimize the planning strategy as its superiority compared to other conventional and optimization algorithms, as previously highlighted in the literatures [17] and [54]. Hence, the MOGWO algorithm is preferred for its superior convergence rate, computational efficiency, and robustness against stochastic variations, making it more suitable for solving the complex optimization problem in RESs compared to other algorithms such as PSO and GA. Therefore, it is used to optimize the best size and placement of PVs and ESSs at each partition area according to the objective function to enhance the power quality and increase the HC of the studied system. The planning strategy involves two operation stages, as summarized:

- **Stage 1: Single Allocation Process**

This stage is responsible for identifying the best candidate buses in each zone for the implementation of PVs and ESSs. It involves randomly selecting the locations and sizes within each zone individually (one zone is active at a time). The objective function is calculated and minimized, determining the optimal locations for PVs and ESSs in each zone.

- **Stage 2: Multiple Allocation Process**

This stage optimizes the sizes of PVs (kVA) and ESSs (kW, kWh) across all zones simultaneously, based on the best

locations identified in Stage 1. The objective function is again calculated and minimized, resulting in the optimal sizing of PVs and ESSs for each zone. The complete flowchart of the proposed planning strategy is given in Fig.13.

IV. SIMULATION RESULTS

To showcase the effectiveness of the proposed planning strategy, various cases are tested using daily simulation based on the system configuration and data, as stated in section III. These cases are named as,

- **Case 1: results without respecting either PVs or ESSs.**
- **Case 2: results with PVs and ESSs.**

A. OPTIMAL PLACEMENT AND SIZING OF DGS AND ESSS

The MOGWO algorithm is given the best placement and sizing of DGs and ESSs at each zone for case 2, as depicted in Table 7. According to Eq. (18), the penetration level has increased to approximately 150% of the total demand. It is notable that the optimizer selected the best locations for PV systems and ESSs, often installing them on the same bus to mitigate the intermittent of DGs, except in Zone 5. In this zone, a small-sized PV system was installed at a distant bus, while the ESS was placed near the wind-based DG for the same purpose.

B. VOLTAGE VIOLATION IMPROVEMENTS

The installation of both PV systems and ESSs contributes to improved voltage profiles and reduced voltage unbalance at each bus, as depicted in Fig. 14 (a). It is evident that the VUI%

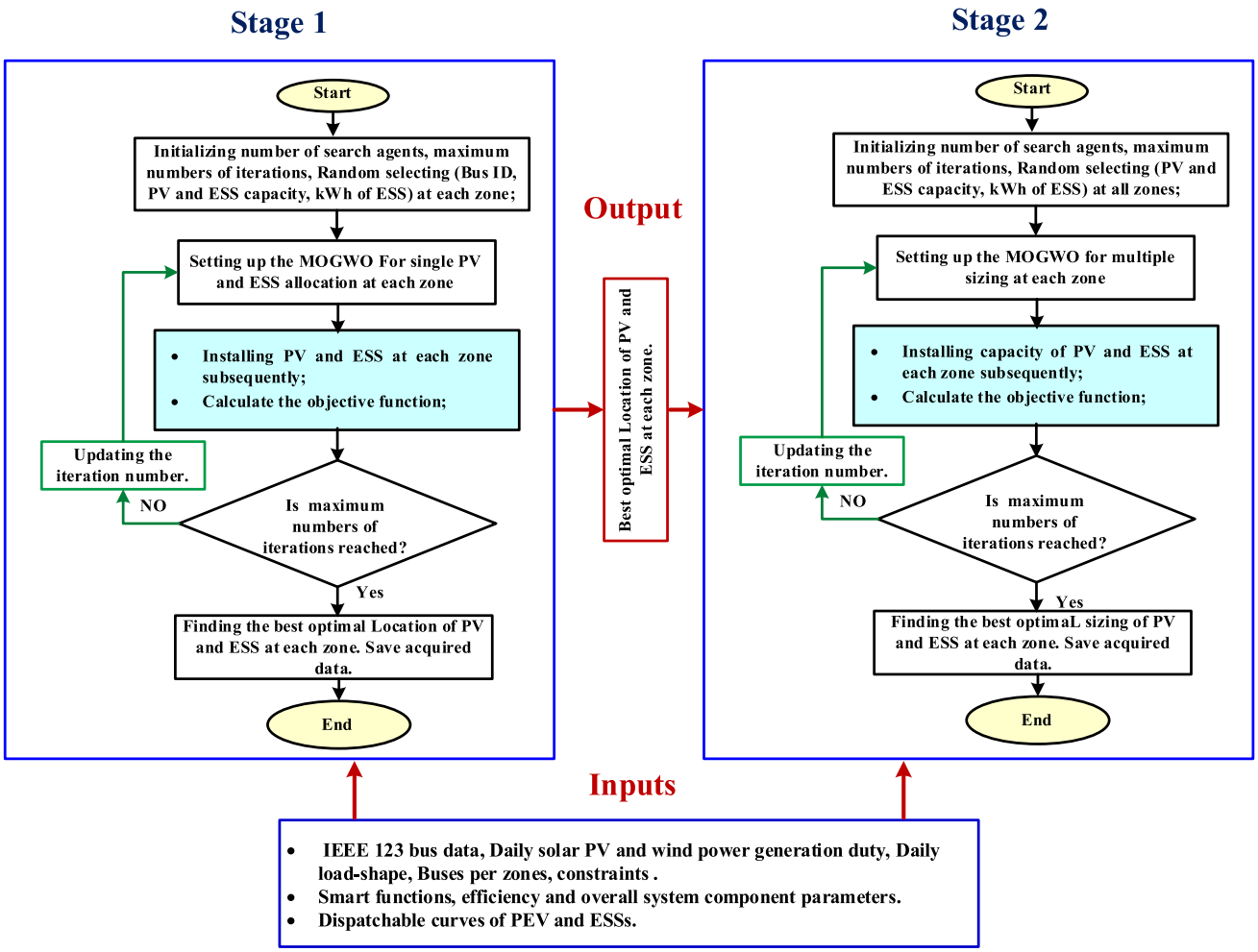

FIGURE 13. Flow chart of optimal planning strategy using the MOGWO.

TABLE 7. Best Allocation results of PVs and ESSs at each zone.

		Z#1	Z#2	Z#3	Z#4	Z#5	Z#6
PV	Bus ID	149	13	35	52	78	101
	kVA	1630	2500	10	2320	40	20
ESS	Bus ID	149	13	35	52	67	101
	kW	1000	500	400	200	400	300
	kWh	4000	2000	2000	1000	2000	1000

decreased in Case 2 compared to Case 1 by 11%. Specifically, the average VUI% of the studied system is 0.810994% in Case 2, compared to 0.910177% in Case 1. The maximum VUI% occurred at buses 30 and 250, with values of 1.4593% and 1.5907% in Case 2 and Case 1, respectively. Conversely, the minimum VUI% in both cases is 0.0002% at bus 149. It is clear that the maximum VUI% does not exceed the standard value of 2% as per EN-50160.

Fig. 14(b) depicts the voltage profile per bus for all candidate buses in Case 2. It is evident that the minimum and maximum voltage levels are between 0.99 pu and 1.039 pu, respectively. Additionally, zones 2, 3, and 4 require more attention to address voltage unbalance problems, while the remaining zones need to decrease voltage rises to reduce voltage deviation. More voltage regulation techniques need to be implemented, as will be discussed in future work.

C. FEEDER CONGESTION AND POWER LOSS REDUCTION

In this section, the results of feeder overloading and power losses are investigated. Accurate deployment planning of both PV systems and ESSs should contribute to reducing losses and overloading in the main feeder of each zone. Tables 8 and 9 provide a summary of selected feeder characteristics, including current congestion under normal and emergency conditions, average current unbalance based on symmetrical current components, and average daily power losses. Key findings from these tables can be summarized as follows:

TABLE 8. Overloading on lines in Case 1.

Feeder	I_{Rate} (A)	I_{avg} (A)	Avg. Overloading		Avg. Emergency condition		Avg. symmetrical current components (A)			Avg. current unbalance		Avg. Power losses		
			Amps. Over	I_{OL}%	I_{em} (A), rated	%I_{max}/I_{em}	I_1	I_2	I_0	%I_2/I_1	%I_0/I_1	P (kW)	Q (kvar)	Avg. P_{loss} %
Line#115	400	467	159	138	600	92	466	53	44	12	10	17	36	0.5
Line#13	400	136	226	44	600	29	136	21	17	16	12	3	6	0.33
Line#114	400	94	297	26	600	17	94	12	7	13	8	0.6	1	0.1
Line#116	400	296	128	83	600	55	296	23	18	9	7	7	15	0.3
Line#117	400	126	256	36	600	24	125	16	13	14	12	1	2	0.1
Line#118	400	37	351	12	600	8	37	7	6	18	17	0.1	0.14	0.03

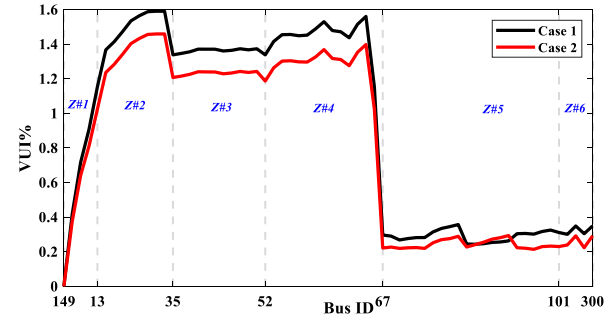

a. Voltage unbalance

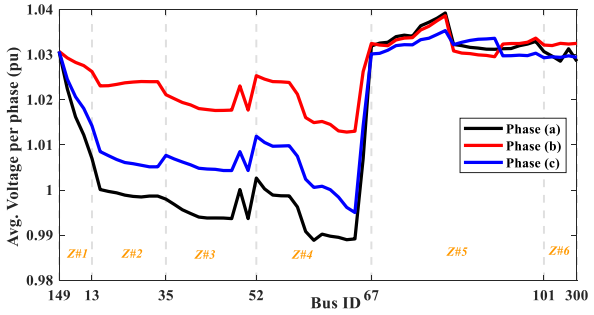

b. Daily average voltage profile per bus in Case 2.

FIGURE 14. Volage violation improvements.

- Improvements in the main feeder (Line #115) are noticeable, with the average overloading per day reduced to 112% in Case 2 compared to 138% in Case 1, meeting the standards set by EN 50160 and VDE-AR-N 4105, which state that overloading should be within 100% or 150% of the nominal feeder rating, respectively. Other feeders showed slight improvements as they were not overloaded. On average, feeder congestion is reduced by 16% by applying the planning strategy.
- For Line #115, the average power losses are reduced to 13 kW and 28 kvar, with an average power loss ratio (Avg. P_{loss} %) of 0.2% per day in Case 2, compared to 17 kW and 36 kvar in Case 1, where the Avg. P_{loss} % is 0.5%.

According to the HC term which refers to the maximum size of total DGs, such as PVs or wind power, that a feeder can accommodate at each zone without compromising power quality or reliability. Ideally, HC should be between 50% and 100% of the feeder capacity based on DSO rules of thumb. The results reveal varying HC utilization across different zones, with some operating near or at capacity limits (zones 1, 2, 4, 5), while others have significant available capacity (zones 3, 6). Attention is needed to increase the HC capacity of zones 3 and 6, especially with the inclusion of wind generation in Zone 5. These findings are crucial for planning future DGs and ESS installations to ensure they remain within feeder HC limits and maintain power quality and system reliability.

Fig.15 (a) and Fig.15 (b) present the total active (P in MW) and reactive (Q in Mvar) power losses of the entire studied system per hour, respectively. Notably, there is a reduction in both components of power losses by 12.77% and 13.66%, respectively, in Case 2, with values of 2.05 MW and 4.11 Mvar, compared to Case 1, which recorded 2.35 MW and 4.76 Mvar. It is observed that the majority of losses occur during the late hours of the day due to increased demand from normal loads and PEVs, without adequate support from DG capacities. As a result, the main power source is provided by the UG, causing more losses and overloading in the main feeders.

D. RESULTS OF INTEGRATED DGS AND ESSS

In Fig. 16, the injected electrical power generated from the WT is depicted. It is notable that when the wind speed is below the cut-in speed, the generated power is zero, such as at hour 8. Conversely, when the wind speed exceeds the cut-out speed, the generated power is limited to the rated power, as previously discussed.

In Fig. 17 (a,b), the injected active power and absorbed reactive power are shown for each PV deployed in each zone, respectively. It is worth mentioning that the smart functions of inverters regulated the power exchange between the PVs and connected buses according to the voltage of the main feeders in each zone. In Fig.17 (a), the active power is regulated using the VW mode, which curtails the generated power to the maximum value when the voltage of the main feeder is between 1 pu and 1.02 pu, as observed in PV1, PV5, and PV6. Additionally, the VV mode operates to serve the same

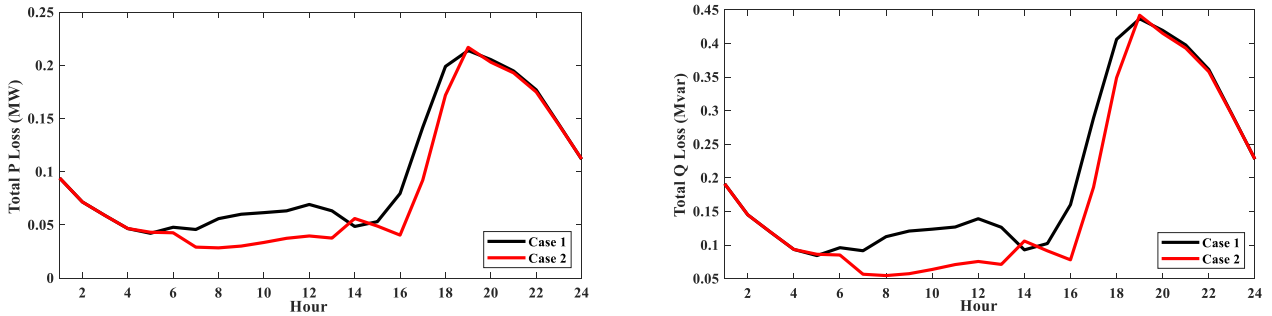

a. Active power loss. b. Reactive power loss.

FIGURE 15. Total power loss of the studied system.

TABLE 9. Overloading on lines in Case 2.

Feeder	I_{Rate} (A)	I_{avg} (A)	Avg. Overloading		Avg. Emergency condition		Avg. symmetrical current components (A)			Avg. current unbalance		Avg. Power losses			HC limits	
			Amps. Over	I_{OL}%	I_{em} (A), rated	%I_{max} /I_{em}	I_1	I_2	I_0	%I_2/ I_1	%I_0/ I_1	P (kW)	Q (kvar)	Avg. P_{loss} %	Feeder HC	Installed
Line#115	400	392	192	112	600	75	389	51	43	16	14	13	28	0.2	100 %	65.2%
Line#13	400	138	224	44	600	29	137	21	17	15	12	3	6	0.33	100 %	100%
Line#114	400	95	294	26	600	18	96	12	7	13	7	0.6	1	0.1	100 %	0.4%
Line#116	400	239	180	66	600	44	238	22	18	16	13	6	12	0.3	100 %	92.8%
Line#117	400	126	250	36	600	24	125	16	13	14	11	1	2	0.2	100 %	61.6%
Line#118	400	39	349	13	600	8	39	7	6	17	17	0.1	0.14	0.03	100 %	0.8%

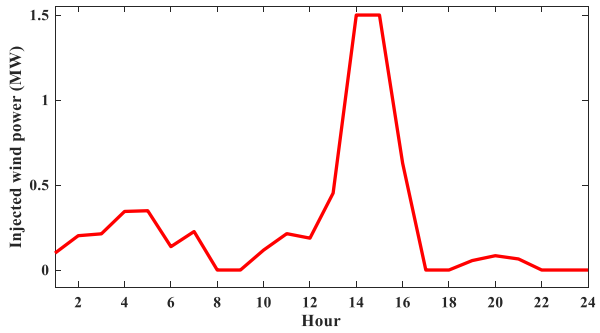

FIGURE 16. Generated wind power.

purpose when the voltage exceeds 1 pu, where the maximum reactive power is absorbed, constrained by the size of the equipped PV in each zone, as depicted in Fig.17 (b).

For further clarification on the smart functions of inverters, the combined VV-VW mode operation is shown in Fig.18 (a,b), with respect to the average operating voltage of the equipped buses for PV1 and PV6. It is worth noting that the operation period for both VV and VW modes is between hour 5 and hour 20, which corresponds to the limited generation period for the PVs. Additionally, it is clear that these modes observe the average voltage and compare it with reference values to regulate it to the desired V_{reg} value.

Fig.19 (a,b) depicts the dispatchable power and energy of all ESSs in the studied system, respectively. As observed, the operation of the ESSs follows the dispatchable curve as mentioned previously. The charging and discharging processes continue until the maximum capacity of the ESSs is reached in each mode. However, this capacity is not applicable for all ESSs, and therefore, the VW mode of the inverters cannot be activated.

E. POWER BALANCE AND GRID DEPENDENCY

In Case 1, the required active and reactive powers are imported from the UG in the presence of wind energy, as depicted in Fig.20 (a,b). In Fig. 21, the power balance in Case 2 is shown in terms of active and reactive powers, respectively. In Fig. 21 (a), the active power exchanged is depicted. It is observed that active power is imported from the UG during periods when the PVs are not generating power, which is necessary to meet the demand alongside ESSs and

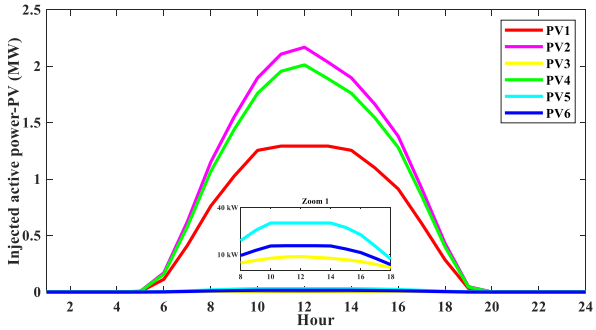

a. Generated active power.

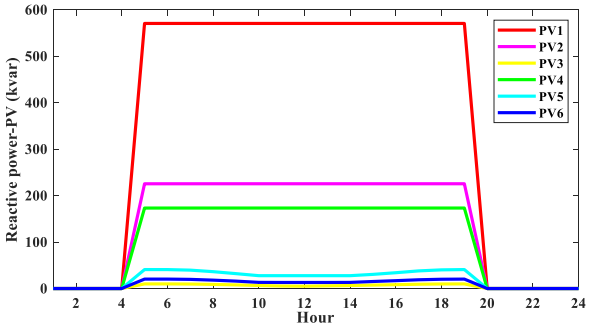

b. Absorbed reactive power.

FIGURE 17. Dispatchable power of PVs.

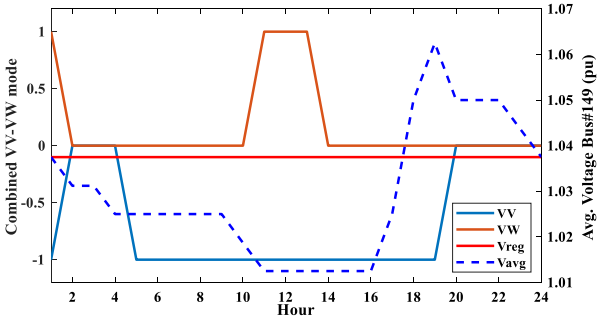

a. Characteristics of PV1.

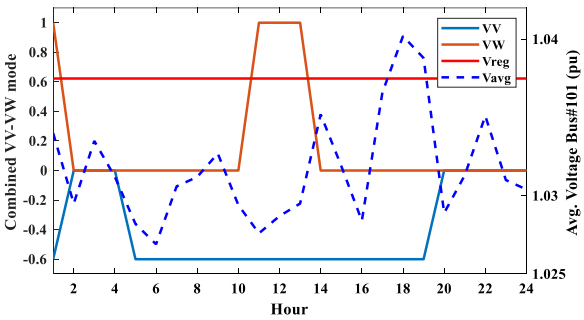

b. Characteristics of PV6.

FIGURE 18. Smart functions of PV inverters.

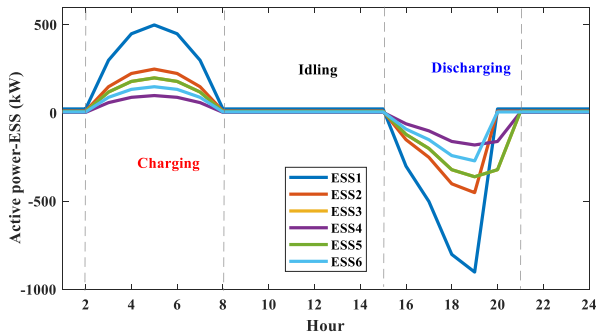

a. Swapped active power.

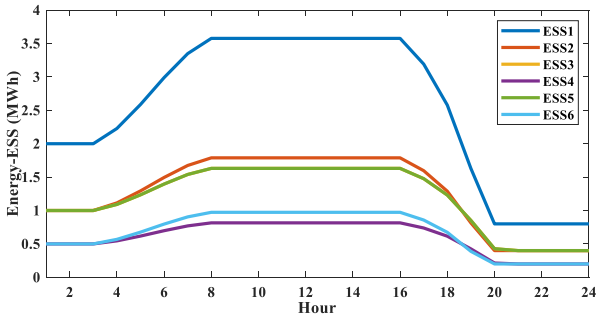

b. Swapped energy.

FIGURE 19. Dispatchable power of ESSs.

wind power. When the PVs start generating power, the excess power is exported to the UG as the ESSs enter an idling mode. Conversely, reactive power is imported from the grid throughout all periods to meet the reactive power requirements of the demand and PVs, ensuring voltage regulation as shown in Fig. 21 (b). The power balance results in Case 2 demonstrate the superiority of integrating both PVs and ESSs in reducing dependency on the UG to support the demands.

F. DISCUSSION

In Table 10, a summary of the daily simulation results of the studied system is provided, highlighting the main findings of applying the proposed planning strategy for deploying PVs and ESSs. These findings can be summarized as follows:

- The MOGWO algorithm effectively placed DGs and ESSs, increasing penetration levels to 150% of total demand.
- Improved voltage profiles and reduced voltage unbalance were observed, with VUI% decreasing by 11% in Case 2.
- Feeder congestion decreased by 16%, and power losses for Line #115 dropped significantly in Case 2.
- Varying HC utilization across zones highlights the need for future planning to optimize capacities.
- The smart functions of inverters effectively operate to regulate the voltage according to the main connected feeder at each zone.
- Integration of PVs and ESSs reduced dependency on the UG, enhancing system reliability and efficiency.

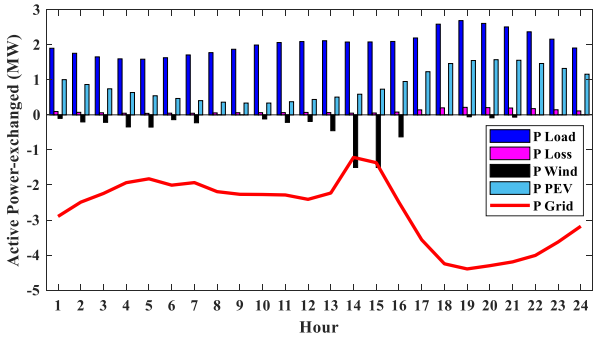

a. Active power.

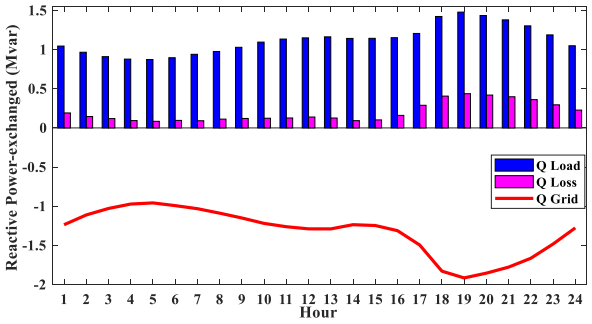

b. Reactive power.

FIGURE 20. Power balance in Case 1.

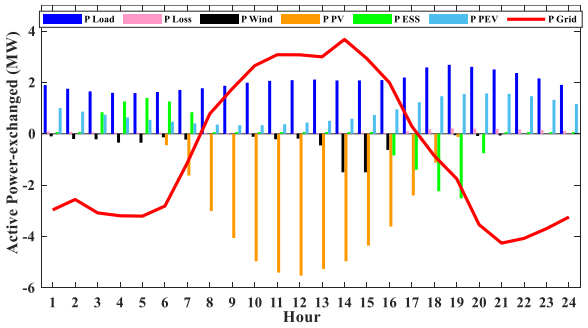

a. Active power.

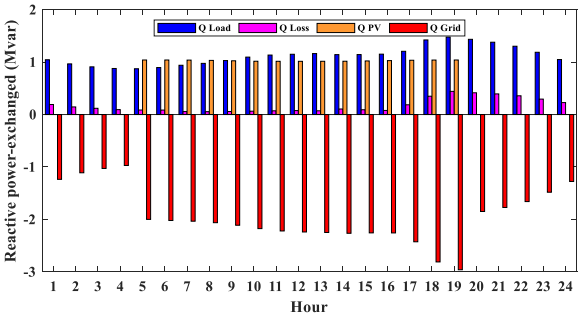

b. Reactive power.

FIGURE 21. Power balance in Case 2.

TABLE 10. Summary of daily simulation results.

		Case 1	Case 2
VUI%	Avg. VUI%	0.910177%	0.810994%
	Max. VUI%	1.5907% at bus#30&250	1.4593% at bus#30&250
	Min. VUI%	0.0002% at bus#149	0.0002% at bus#149
Total Losses	P (MW)	2.35	2.05
	Q (Mvar)	4.76	4.11
Total overloading of feeders	Avg. $\mathbf{I_{OL}}$%	56.5%	47.3%
	Max. $\mathbf{I_{OL}}$%	138% at Line#115	112% at Line#115
	Min. $\mathbf{I_{OL}}$%	12% at Line#118	13% at Line#118
Avg. Voltage (pu)	Min.	0.98 pu at bus#61&66	0.99 pu at bus#61&66
	Max.	1.042 pu at bus#83	1.039 pu at bus#83

Overall, the integration of PVs and ESSs under the proposed planning strategy proved effective in improving voltage profiles, reducing feeder congestion and power losses, and optimizing HC utilization. Future work should focus on further refining voltage regulation techniques and enhancing HC capacities in underutilized zones.

V. CONCLUSION

This article examines the coordinated deployment planning of DGs based on RESs and ESSs within an unbalanced three-phase IEEE 123-bus microgrid. The studied system is segmented into six operational zones, each containing candidate unbalanced three-phase buses for the placement of both PV systems and ESSs. This is done in the context of PEV demand in the residential sector and wind-based DG connected to the end buses. The planning strategy aims to address several key objectives: mitigating voltage unbalance, reducing voltage deviations, decreasing power losses, and alleviating congestion and overloading in the main feeders. Additionally, it seeks to maximize the HC of RESs in a grid-connected unbalanced microgrid to accommodate additional DGs within each partitioned area while minimizing the exchanged power between these areas and the UG. Moreover, smart inverter control functions are employed, including combined mode, VV-VW), for PV inverters, as well as VW for ESS inverters. The study also considers the

uncertainties in demand and generation, incorporating the dispatchable curve of ESSs. To optimize the planning problem, the MOGWO algorithm is utilized using co-simulation between MATLAB and OpenDSS platforms. As a result, the proposed planning strategy led to enhanced power quality, reduced feeder congestion by 16%, increased penetration level of PVs to 150%, and minimized power losses by approximately 13%. Additionally, the results emphasized the importance of adhering to feeder HC limits to maintain system reliability. Furthermore, the successful integration of PVs and ESSs demonstrated a promising approach to reduce dependency on the UG while supporting demands. These results underscore the significance of strategic planning and optimization techniques in advancing the efficiency and resilience of grid-connected unbalanced microgrids.

For future work, sensitivity analysis of various integrated RESs will be conducted, alongside evaluating the robustness of different metaheuristic algorithms. This evaluation will focus on aspects such as convergence rate, computational efficiency, and solution quality across multiple optimization techniques, ensuring a more rigorous assessment of performance. Additionally, sensitivity analysis of objective function weights will be included to further validate the robustness of the proposed approach. In terms of HC estimation and enhancement strategies, advanced voltage violation mitigation will be explored using robust control systems and data-driven approaches, particularly in the presence of PEVs and multi-carrier energy systems (MESs).

CREDIT AUTHORSHIP CONTRIBUTION STATEMENT

Hossam H. H. Mousa: Conceptualization, software, validation, writing-original draft.

Karar Mahmoud: Writing-review and editing, supervision.

Matti Lehtonen: Writing-review and editing, supervision.

DECLARATION OF COMPETING INTEREST

The authors declare that they have no known competing financial interests or personal relationships that could have appeared to influence the work reported in this paper.

DATA AVAILABILITY

Data will be available upon request.

DECLARATION OF AI-ASSISTED TECHNOLOGIES IN THE WRITING PROCESS

During the preparation of this work the authors used AI tools in order to improve language quality and readability. After using these tools/services, the authors reviewed and edited the content as needed and take full responsibility for the content of the publication.

REFERENCES

[1] H. H. H. Mousa, A.-R. Youssef, and E. E. M. Mohamed, "State of the art perturb and observe MPPT algorithms based wind energy conversion systems: A technology review," *Int. J. Electr. Power Energy Syst.*, vol. 126, Mar. 2021, Art. no. 106598.

[2] D. Zhang, G. M. Shafiullah, C. K. Das, and K. W. Wong, "A systematic review of optimal planning and deployment of distributed generation and energy storage systems in power networks," *J. Energy Storage*, vol. 56, Dec. 2022, Art. no. 105937, doi: 10.1016/j.est.2022.105937.

[3] *Modern Renewable Energy Generation By Source, World*. Accessed: Jun. 03, 2024. [Online]. Available: https://ourworldindata.org/grapher/modern-renewable-prod

[4] D. A. Quijano and A. Padilha-Feltrin, "Optimal integration of distributed generation and conservation voltage reduction in active distribution networks," *Int. J. Electr. Power Energy Syst.*, vol. 113, pp. 197–207, Dec. 2019, doi: 10.1016/j.ijepes.2019.05.039.

[5] E. S. Oda, M. Ebeed, A. M. Abd El Hamed, A. Ali, A. A. Elbaset, and M. Abdelsattar, "Optimal allocation of a hybrid photovoltaic-basedDGandDSTATCOMunder the load and irradiance variability," *Int. Trans. Electr. Energy Syst.*, vol. 31, no. 11, p. 13131, Nov. 2021, doi: 10.1002/2050-7038.13131.

[6] B. Tan, J. Zhao, M. Netto, V. Krishnan, V. Terzija, and Y. Zhang, "Power system inertia estimation: Review of methods and the impacts of converter-interfaced generations," *Int. J. Electr. Power Energy Syst.*, vol. 134, Jan. 2022, Art. no. 107362, doi: 10.1016/j.ijepes.2021.107362.

[7] A. Ali, H. H. H. Mousa, M. F. Shaaban, M. A. Azzouz, and A. S. A. Awad, "A comprehensive review on charging topologies and power electronic converter solutions for electric vehicles," *J. Modern Power Syst. Clean Energy*, vol. 12, no. 3, pp. 675–694, 2024, doi: 10.35833/mpce.2023.000107.

[8] F. Lezama, J. Soares, B. Canizes, and Z. Vale, "Flexibility management model of home appliances to support DSO requests in smart grids," *Sustain. Cities Soc.*, vol. 55, Apr. 2020, Art. no. 102048, doi: 10.1016/j.scs.2020.102048.

[9] Z. A. Arfeen, M. P. Abdullah, R. Hassan, B. M. Othman, A. Siddique, A. U. Rehman, and U. U. Sheikh, "Energy storage usages: Engineering reactions, economic-technologicalvalues for electric vehicles—A technological outlook," *Int. Trans. Electr. Energy Syst.*, vol. 30, no. 9, p. 12422, Sep. 2020, doi: 10.1002/2050-7038.12422.

[10] L. A. Wong, V. K. Ramachandaramurthy, P. Taylor, J. B. Ekanayake, S. L. Walker, and S. Padmanaban, "Review on the optimal placement, sizing and control of an energy storage system in the distribution network," *J. Energy Storage*, vol. 21, pp. 489–504, Feb. 2019, doi: 10.1016/j.est.2018.12.015.

[11] A. Ali, K. Mahmoud, and M. Lehtonen, "Maximizing hosting capacity of uncertain photovoltaics by coordinated management of OLTC, VAr sources and stochastic EVs," *Int. J. Electr. Power Energy Syst.*, vol. 127, May 2021, Art. no. 106627, doi: 10.1016/j.ijepes.2020.106627.

[12] H. H. H. Mousa, K. Mahmoud, and M. Lehtonen, "A comprehensive review on recent developments of hosting capacity estimation and optimization for active distribution networks," *IEEE Access*, vol. 12, pp. 18545–18593, 2024, doi: 10.1109/ACCESS.2024.3359431.

[13] A. Rastgou, "Distribution network expansion planning: An updated review of current methods and new challenges," *Renew. Sustain. Energy Rev.*, vol. 189, Jan. 2024, Art. no. 114062, doi: 10.1016/j.rser.2023.114062.

[14] V. Pattanaik, B. K. Malika, S. Mohanty, P. K. Rout, and B. K. Sahu, "Optimal energy storage allocation in smart distribution systems: A review," in *Lecture Notes in Networks and Systems*. Cham, Switzerland: Springer, 2021, pp. 555–565.

[15] L. Grisales-Noreña, B. Restrepo-Cuestas, B. Cortés-Caicedo, J. Montano, A. Rosales-Muñoz, and M. Rivera, "Optimal location and sizing of distributed generators and energy storage systems in microgrids: A review," *Energies*, vol. 16, no. 1, p. 106, Dec. 2022, doi: 10.3390/en16010106.

[16] S. M. Tercan, A. Demirci, Y. E. Unutmaz, O. Elma, and R. Yumurtaci, "A comprehensive review of recent advances in optimal allocation methods for distributed renewable generation," *IET Renew. Power Gener.*, vol. 17, no. 12, pp. 3133–3150, Sep. 2023, doi: 10.1049/rpg2.12815.

[17] A. Rezaee. Jordehi, "DG allocation and reconfiguration in distribution systems by metaheuristic optimisation algorithms: A comparative analysis," in *Proc. IEEE PES Innov. Smart Grid Technol. Conf. Eur. (ISGT-Europe)*, Oct. 2018, pp. 1–6, doi: 10.1109/ISGTEUROPE.2018.8571802.

[18] S. Jothibasu, A. Dubey, and S. Santoso, "Two-stage distribution circuit design framework for high levels of photovoltaic generation," *IEEE Trans. Power Syst.*, vol. 34, no. 6, pp. 5217–5226, Nov. 2019, doi: 10.1109/TPWRS.2018.2871640.

[19] M. Mahdavi, A. Awaafo, K. Schmitt, M. Chamana, F. Jurado, and S. Bayne, "An effective formulation for minimizing distribution network costs through distributed generation allocation in systems with variable loads," *IEEE Trans. Ind. Appl.*, vol. 60, no. 4, pp. 5671–5680, Jul. 2024, doi: 10.1109/tia.2024.3382255.

[20] M. Abdelaziz and M. Moradzadeh, "Monte-carlo simulation based multi-objective optimum allocation of renewable distributed generation using OpenCL," *Electric Power Syst. Res.*, vol. 170, pp. 81–91, May 2019, doi: 10.1016/j.epsr.2019.01.012.

[21] A. Pal, A. Bhattacharya, and A. K. Chakraborty, "Placement of public fast-charging station and solar distributed generation with battery energy storage in distribution network considering uncertainties and traffic congestion," *J. Energy Storage*, vol. 41, Sep. 2021, Art. no. 102939, doi: 10.1016/j.est.2021.102939.

[22] S. Zambrano-Asanza, J. Quiros-Tortos, and J. F. Franco, "Optimal site selection for photovoltaic power plants using a GIS-based multi-criteria decision making and spatial overlay with electric load," *Renew. Sustain. Energy Rev.*, vol. 143, Jun. 2021, Art. no. 110853, doi: 10.1016/j.rser.2021.110853.

[23] C. Venkatesan, R. Kannadasan, M. H. Alsharif, M.-K. Kim, and J. Nebhen, "A novel multiobjective hybrid technique for siting and sizing of distributed generation and capacitor banks in radial distribution systems," *Sustainability*, vol. 13, no. 6, p. 3308, Mar. 2021, doi: 10.3390/su13063308.

[24] S. O. Ayanlade, F. K. Ariyo, A. Jimoh, K. T. Akindeji, A. O. Adetunji, E. I. Ogunwole, and D. E. Owolabi, "Optimal allocation of photovoltaic distributed generations in radial distribution networks," *Sustainability*, vol. 15, no. 18, p. 13933, Sep. 2023, doi: 10.3390/su151813933.

[25] M. Khasanov, S. Kamel, E. H. Houssein, C. Rahmann, and F. A. Hashim, "Optimal allocation strategy of photovoltaic- and wind turbine-based distributed generation units in radial distribution networks considering uncertainty," *Neural Comput. Appl.*, vol. 35, no. 3, pp. 2883–2908, Sep. 2022, doi: 10.1007/s00521-022-07715-2.

[26] A. Ramadan, M. Ebeed, S. Kamel, E. M. Ahmed, and M. Tostado-Véliz, "Optimal allocation of renewable DGs using artificial hummingbird algorithm under uncertainty conditions," *Ain Shams Eng. J.*, vol. 14, no. 2, Mar. 2023, Art. no. 101872, doi: 10.1016/j.asej.2022.101872.

[27] M. Cikan and N. N. Cikan, "Optimum allocation of multiple type and number of DG units based on IEEE 123-bus unbalanced multiphase power distribution system," *Int. J. Electr. Power Energy Syst.*, vol. 144, Jan. 2023, Art. no. 108564, doi: 10.1016/j.ijepes.2022.108564.

[28] B. Mukhopadhyay and D. Das, "Multi-objective dynamic and static reconfiguration with optimized allocation of PV-DG and battery energy storage system," *Renew. Sustain. Energy Rev.*, vol. 124, May 2020, Art. no. 109777, doi: 10.1016/j.rser.2020.109777.

[29] M. Khasanov, S. Kamel, C. Rahmann, H. M. Hasanien, and A. Al-Durra, "Optimal distributed generation and battery energy storage units integration in distribution systems considering power generation uncertainty," *IET Gener., Transmiss. Distrib.*, vol. 15, no. 24, pp. 3400–3422, Dec. 2021, doi: 10.1049/gtd2.12230.

[30] J. Liao, J. Lin, and G. Wu, "Two-layer optimization configuration method for distributed photovoltaic and energy storage systems based on IDEC-K clustering," *Energy Rep.*, vol. 11, pp. 5172–5188, Jun. 2024, doi: 10.1016/j.egyr.2024.04.047.

[31] M. Z. Oskouei, B. Mohammadi-Ivatloo, O. Erdinç, and F. G. Erdinç, "Optimal allocation of renewable sources and energy storage systems in partitioned power networks to create supply-sufficient areas," *IEEE Trans. Sustain. Energy*, vol. 12, no. 2, pp. 999–1008, Apr. 2021, doi: 10.1109/TSTE.2020.3029104.

[32] S. S. K. R. Vaka and S. K. Matam, "Optimal sizing and management of battery energy storage systems in microgrids for operating cost minimization," *Electr. Power Compon. Syst.*, vol. 49, nos. 16–17, pp. 1319–1332, Oct. 2021, doi: 10.1080/15325008.2022.2061641.

[33] T. Adefarati, R. C. Bansal, M. Bettayeb, and R. Naidoo, "Optimal energy management of a PV-WTG-BSS-DG microgrid system," *Energy*, vol. 217, Feb. 2021, Art. no. 119358, doi: 10.1016/j.energy.2020.119358.

[34] X. Li and G. Jones, "Optimal sizing, location, and assignment of photovoltaic distributed generators with an energy storage system for islanded microgrids," *Energies*, vol. 15, no. 18, p. 6630, Sep. 2022, doi: 10.3390/en15186630.

[35] A. Ghaffari, A. Askarzadeh, and R. Fadaeinedjad, "Optimal allocation of energy storage systems, wind turbines and photovoltaic systems in distribution network considering flicker mitigation," *Appl. Energy*, vol. 319, Aug. 2022, Art. no. 119253, doi: 10.1016/j.apenergy.2022.119253.

[36] T. Gu, P. Wang, F. Liang, G. Xie, L. Guo, X.-P. Zhang, and F. Shi, "Placement and capacity selection of battery energy storage system in the distributed generation integrated distribution network based on improved NSGA-II optimization," *J. Energy Storage*, vol. 52, Aug. 2022, Art. no. 104716, doi: 10.1016/j.est.2022.104716.

[37] N. B. Roy and D. Das, "Probabilistic optimal power allocation of dispatchable DGs and energy storage units in a reconfigurable grid-connected CCHP microgrid considering demand response," *J. Energy Storage*, vol. 72, Nov. 2023, Art. no. 108207, doi: 10.1016/j.est.2023.108207.

[38] B. Azibek, N. Zhakiyev, A. Kushekkaliyev, A. Zhalgas, and B. Mukatov, "Optimal allocation of storage capacity in distribution network for renewable energy expansion," *Electr. Power Compon. Syst.*, vol. 52, no. 10, pp. 1749–1762, Jun. 2024, doi: 10.1080/15325008.2023.2276835.

[39] *Resources—IEEE PES Test Feeder*. Accessed: Mar. 28, 2024. [Online]. Available: https://cmte.ieee.org/pes-testfeeders/resources/

[40] A. I. M. Ali, H. H. H. Mousa, H. R. A. Mohamed, S. Kamel, A. S. Hassan, Z. M. Alaas, E. E. M. Mohamed, and A.-R.-Y. Abdallah, "An enhanced P&O MPPT algorithm with concise search area for grid-tied PV systems," *IEEE Access*, vol. 11, pp. 79408–79421, 2023, doi: 10.1109/access.2023.3298106.

[41] H. Rezk and A. Fathy, "Hydrogen reduction-based energy management strategy of hybrid fuel cell/PV/battery/supercapacitor renewable energy system," *J. Energy Storage*, vol. 86, May 2024, Art. no. 111316, doi: 10.1016/j.est.2024.111316.

[42] *IEEE Standard for Interconnection and Interoperability of Distributed Energy Resources With Associated Electric Power Systems Interfaces*, IEEE Standard 1547-2018, 2018, pp. 1–138.

[43] S. M. S. Ullah, S. Ebrahimi, F. Ferdowsi, and M. Barati, "Techno-economic impacts of volt-VAR control on the high penetration of solar PV interconnection," *Cleaner Energy Syst.*, vol. 5, Aug. 2023, Art. no. 100067, doi: 10.1016/j.cles.2023.100067.

[44] D. C. Montgomery, *Applied Statistics and Probability for Engineers*, vol. 4, 7th ed., Hoboken, NJ, USA: Wiley.

[45] M. U. Afzaal, I. A. Sajjad, A. B. Awan, K. N. Paracha, M. F. N. Khan, A. R. Bhatti, M. Zubair, W. U. Rehman, S. Amin, S. S. Haroon, R. Liaqat, W. Hdidi, and I. Tlili, "Probabilistic generation model of solar irradiance for grid connected photovoltaic systems using Weibull distribution," *Sustainability*, vol. 12, no. 6, p. 2241, Mar. 2020, doi: 10.3390/su12062241.

[46] O. M. Kam, S. Noel, H. Ramenah, P. Kasser, and C. Tanougast, "Comparative Weibull distribution methods for reliable global solar irradiance assessment in France areas," *Renew. Energy*, vol. 165, pp. 194–210, Mar. 2021, doi: 10.1016/j.renene.2020.10.151.

[47] C.-T. Pham. *Assessment of Energy Storage Systems for Power System Applications Based on Equivalent Circuit Modeling*. [Online]. Available: https://kth.diva-portal.org/smash/record.jsf?pid=diva2%3A1269847&dswid=2008

[48] H. H. H. Mousa, A.-R. Youssef, and E. E. M. Mohamed, "Hybrid and adaptive sectors P&O MPPT algorithm based wind generation system," *Renew. Energy*, vol. 145, pp. 1412–1429, Jan. 2020.

[49] *NREL National Wind Technology Center (NWTC): M2 Tower; Boulder, Colorado (Data) | NREL Data Catalog*. Accessed: May 21, 2024. [Online]. Available: https://data.nrel.gov/submissions/33

[50] Y. Zheng, Z. Y. Dong, K. Meng, H. Yang, M. Lai, and K. P. Wong, "Multi-objective distributed wind generation planning in an unbalanced distribution system," *CSEE J. Power Energy Syst.*, vol. 3, no. 2, pp. 186–195, Jun. 2017, doi: 10.17775/CSEEJPES.2017.0023.

[51] X. Chen, W. Dong, and Q. Yang, "Robust optimal capacity planning of grid-connected microgrid considering energy management under multi-dimensional uncertainties," *Appl. Energy*, vol. 323, Oct. 2022, Art. no. 119642, doi: 10.1016/j.apenergy.2022.119642.

[52] S. Zhou, Y. Han, K. Mahmoud, M. M. F. Darwish, M. Lehtonen, P. Yang, and A. S. Zalhaf, "A novel unified planning model for distributed generation and electric vehicle charging station considering multi-uncertainties and battery degradation," *Appl. Energy*, vol. 348, Oct. 2023, Art. no. 121566, doi: 10.1016/j.apenergy.2023.121566.

[53] K. M. S. Alzaidi, O. Bayat, and O. N. Uçan, "Multiple DGs for reducing total power losses in radial distribution systems using hybrid WOA-SSA algorithm," *Int. J. Photoenergy*, vol. 2019, pp. 1–20, Mar. 2019, doi: 10.1155/2019/2426538.

[54] S. Mirjalili, S. Saremi, S. M. Mirjalili, and L. D. S. Coelho, "Multi-objective grey wolf optimizer: A novel algorithm for multi-criterion optimization," *Expert Syst. Appl.*, vol. 47, pp. 106–119, Apr. 2016, doi: 10.1016/j.eswa.2015.10.039.

HOSSAM H. H. MOUSA received the B.Sc. and M.Sc. degrees in electrical power and machines engineering from South Valley University, Egypt, in 2017 and 2020, respectively. He is currently a Ph.D. Researcher with the Department of Electrical Engineering and Automation, School of Electrical Engineering, Aalto University, Finland. He is also an Assistant Lecturer with the Department of Electrical Engineering, South Valley University, where he started as a Teaching Assistant, in 2018. He has authored or co-authored several publications in top-ranked journals and international conferences. His research interests include electrical power engineering, maximum power point tracking (MPPT) techniques for renewable energy systems, power systems, energy management, applied machine learning, and control systems. His current research focuses on hosting capacity estimation and optimization using machine learning techniques for modern power systems.

KARAR MAHMOUD (Senior Member, IEEE) was a Research Fellow with the Group of Prof. M. Lehtonen, Department of EEA, School of Electrical Engineering, Aalto University, Finland, from 2019 to 2023. He is currently an Associate Professor with the Department of Electrical Engineering, Aswan University, Egypt. He has authored or co-authored several publications in top-ranked journals, including IEEE journals, international conferences, and book chapters. His research interests include power systems, renewable energies, smart grids, energy storage, and distributed generation. He was awarded the Prestigious Egyptian State Encouragement Award in the field of engineering sciences, in 2021, and honored by Egypt's Academy of Scientific Research and Technology (ASRT). He holds the position of topic editor in four classified scientific journals, in addition to being the guest editor for more than ten special scientific issues on advanced scientific engineering topics.

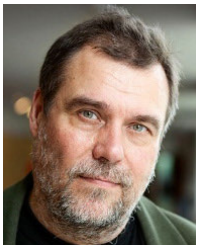

MATTI LEHTONEN received the master's and Licentiate degrees in electrical engineering from Helsinki University of Technology (nowadays Aalto University), in 1984 and 1989, respectively, and the Ph.D. degree in technology from Tampere University of Technology, in 1992. He was with VTT Energy, Espoo, Finland, from 1987 to 2003. Since 1999, he has been a Professor with Aalto University, where he is currently the Head of Power Systems and High Voltage Engineering. His research interests include power system planning and asset management, power system protection, including earth fault problems, harmonic related issues, and the applications of information technology in distribution systems.